Please cite this article in press as: Takahasi et al., Nonself RNA-Sensing Mechanism of RIG-I Helicase and Activation of Antiviral Immune Responses, Molecular Cell (2008), doi:10.1016/j.molcel.2007.11.028

Table 1. Structural Statistics for 20 RIG-I CTD

NOE distance constraints	
Total	2366
Short range $\|i-j\| \leq 1$	1342
Medium range $1 < \|i-j\| < 5$	271
Long range $\|i-j\| \geq 5$	753
Dihedral angle constraints	
phi	79
psi	83
Residual NOE violations	
Number > 0.3	2
Maximum (Å)	0.33
Residual angle violations	
Number > 5.0°	0
Ramachandran statistics (%)	
Residues in most favored regions	73
Residues in additional allowed regions	26.2
Residues in generously allowed regions	0.5
Residues in disallowed regions	0.2
Structural coordinates rmsd (Å) (residues 806–845, 860–915)	
Backbone atoms for the final ensemble	0.63
All heavy atoms for the final ensemble	1.15

Effect of Amino Acid Substitutions on the Function of RIG-I CTD

To confirm the involvement of the CTD cleft in the recognition of nonself RNA, a series of point mutants in the context of full-length RIG-I were generated, expressed in 293T cells, and subjected to RNA-binding assays (Figures 6A and 6B). The wild-type and mutant RIG-I tested were produced at comparable levels in 293T cells (our unpublished data). Binding to dsRNA was not affected by K849A, whereas it was significantly impaired by the KK858/861AA mutation at the bottom of the cleft. A mutation at one edge of the cleft, KK888/907AA, also inactivated dsRNA binding. KK878/880AA, which is distal from the cleft, caused partial inhibition of dsRNA binding. Interestingly, a similar result was obtained for binding with 5′ppp ssRNA. These results not only confirm the importance of the basic cleft but also suggest the involvement of a larger surface for the recognition of nonself RNA species.

Next, we assessed the signaling function of RIG-I mutants by adding them back to *RIG-I*$^{-/-}$ MEFs and stimulating these cells with dsRNA or 5′ppp ssRNA (Figures 6C and 6D). Consistent with the RNA-binding properties of the mutants, KK858/861AA and KK888/907AA are incapable of complementing RIG-I function, whereas R849A, which normally recognizes ligand RNAs, efficiently restored RIG-I's function. The partial RNA-binding mutant KK878/880AA partially retained reactivity to dsRNA and 5′ppp ssRNA. In summary, the results of mutagenesis are consistent with our hypothesis that the basic cleft is responsible for the recognition and triggering of antiviral signaling. It is worth noting that although RIG-I CTD interacts with the helicase linker region (Figure 3E), none of the RNA binding-deficient mutants exhibited constitutive activation of the signal, suggesting that the RNA-sensing surface of CTD is independent of the RD function.

Finally, we investigated the binding properties of poly I:C and RIG-I. RIG-I was subjected to EMSA using ^{32}P-labeled poly I:C as a probe, and binding was competed by a 1600-fold molar excess of various cold RNA (Figure 6E). Although efficient competition was observed with poly I:C, short dsRNA or 5′ppp ssRNA failed to exhibit competition under these conditions. When ^{32}P-labeled short dsRNA was used as a probe, poly I:C efficiently competed binding (Figure 6F). These results suggest that poly I:C, short dsRNA, and 5′ppp ssRNA bind with RIG-I at overlapping sites but poly I:C exhibits significantly higher affinity. We hypothesized that poly I:C interacts with an additional site on RIG-I, presumably with the helicase domain. There are several conserved motifs within the helicase domain, such as TAS (amino acid residues 409 to 410), which is implicated in the unwinding reaction (Pause and Sonenberg, 1992). EMSA was performed using wild-type RIG-I and a mutant of the TAS motif (TS409/411AA) using ^{32}P-labeled poly I:C or short dsRNA (ds25/25c) (Figure 6G). Disruption of the TAS motif apparently impaired binding with poly I:C, whereas binding with short dsRNA was unaffected, suggesting that poly I:C interacts with additional sites, including the TAS motif of the helicase domain.

DISCUSSION

RNA-Binding and Helicase Activity of RIG-I

We produced a full-length recombinant RIG-I, purified it to homogeneity, and subjected it to biochemical analyses. First, we found that dsRNA and 5′ppp ssRNA bound to RIG-I in a competitive manner; however, binding to dsDNA or 5′OH ssRNA was undetectable. Our analysis revealed that dsRNA, relatively small in size, binds to RIG-I independent of a phosphorylated structure or overhang. By contrast, with 5′ppp ssRNA, the 5′ppp structure is critical for recognition, as dephosphorylated or chemically synthesized 5′OH ssRNA failed to bind to RIG-I (Figure 1) (Hornung et al., 2006; Pichlmair et al., 2006). Furthermore, ssRNA with 5′ mono- or diphosphate (including commercial poly rA, which was synthesized by ADP and polynucleotide phosphorylase) does not bind to RIG-I (Yoneyama et al., 2004 and Figure S2).

As predicted from its primary structure, we confirmed that RIG-I is a ligand-dependent ATPase. ATPase activity is induced by binding with various dsRNAs, including poly I:C; however, ATPase activity per se is not perfectly correlated with IFN-inducing signaling. Poly I:C does not activate RIG-I in vivo, and a particular p-dsRNA, 47/25c, induces ATPase efficiently (Figure S5) but failed to activate RIG-I to activate the IFN promoter (Figure 2A).

RIG-I exhibits apparent helicase activity toward dsRNA and RNA/DNA duplexes with a 3′ RNA overhang, indicating a clear structural requirement, the 3′ RNA overhang. RNAs with a blunt end or 5′ overhang were resistant to unwinding by RIG-I. Previously, an opposite result was reported that blunt-end RNA is a better substrate for RIG-I helicase and efficiently induces IFN in cells (Marques et al., 2006). This discrepancy is likely due to the use of a truncated RIG-I and nonoptimal assay conditions that led to inefficient unwinding. Using a series of dsRNAs, which differ in their susceptibility to unwinding by RIG-I, we found a reverse correlation between IFN-inducing potential upon the transfection of cultured cells and susceptibility to unwinding. As in vitro binding suggests (Figure 1G), this is presumably

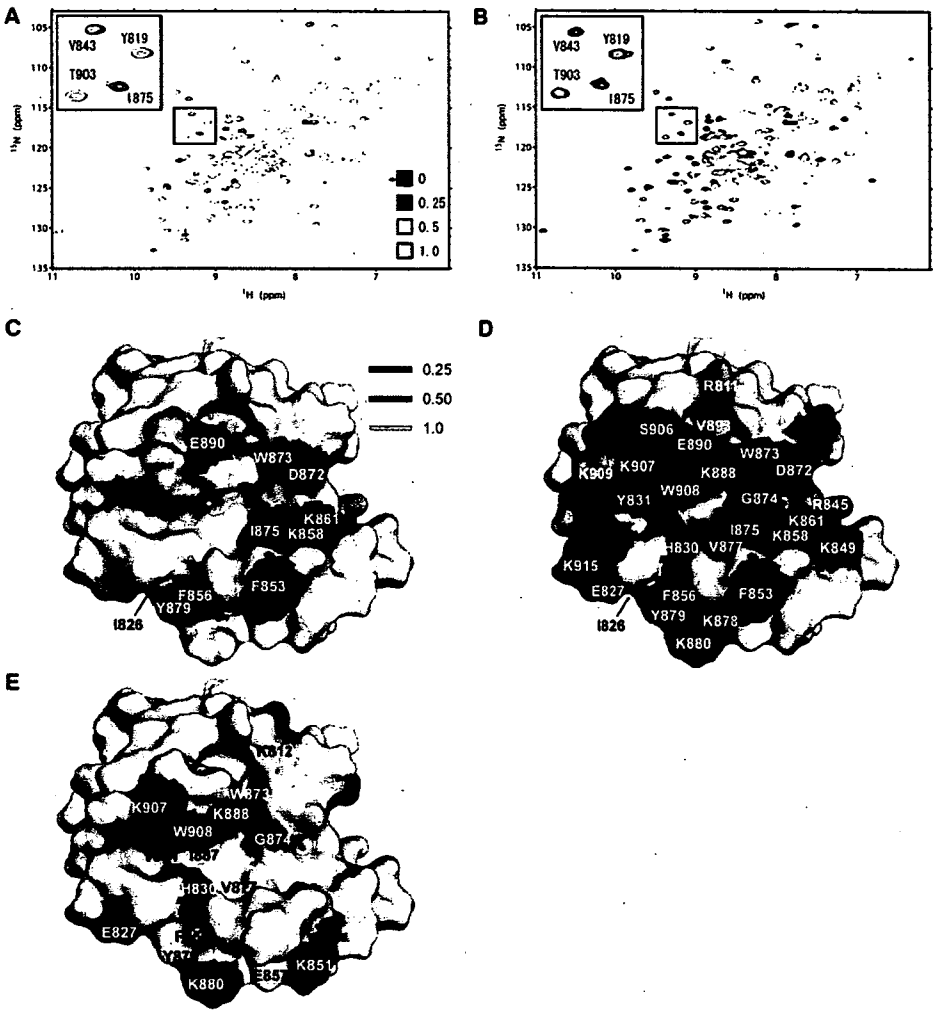

Figure 5. NMR Titration of RIG-I CTD

(A and B) NMR titration of RIG-I CTD with (A) GG25/2+25C and (B) 5′pppGG25. An overlay of ^{1}H-^{15}N-HSQC spectra is shown in blue at 0 equivalents (molar ratio of RNA to RIG-I CTD) and in yellow at 0.5 equivalents. The insert shows additional spectra at 0.25 equivalents in magenta and 1.0 equivalent in cyan. Signal intensity was normalized using the signal derived from the GST tag.

(C) dsRNA-binding site of RIG-I CTD determined from the NMR titration. Residues whose peaks on the spectrum disappeared at 0.25, 0.5, and 1.0 equivalent are shown in blue, sea blue, and light blue, respectively. Residues that disappeared with the addition of 0.5 equivalent of RNA are labeled.

(D) 5′ppp ssRNA-binding site of RIG-I CTD. The same colors as in (C) were used. Residues that disappeared with the addition of 0.25 equivalent of RNA and Lys and Arg residues that disappeared with up to 1 equivalent molar of RNA are labeled.

(E) The conserved residues are colored on the surface of RIG-I CTD. Residues completely conserved among RIG-I, MDA5, and LGP2 are in red, whereas type-conserved residues are in yellow.

because good helicase substrates readily unwound and the RIG-I/dsRNA complex is not stable in cells, whereas the resistant dsRNA/RIG-I complex may exist stably in cells to facilitate persistent interaction with interferon promoter stimulator-1 (IPS-1). The RNA/DNA duplex 47/D25cP, which possesses a 3′ overhang, is unwound by RIG-I as efficiently as the dsRNA substrate (Figure 1F); however, its 5′ overhang variant, 5-47/D25cP, was incapable of inducing IFN gene expression (Figure 2B). This is partly explained by the knowledge that 5-47/D25cP does not exhibit appreciable binding to RIG-I (Figure S4).

Although it has been proposed that large dsRNA is required to efficiently induce the production of IFN (Joklik, 1991), when transfected into cultured cells, dsRNA as small as 25 bp, possessing a 5′- or 3′-monophosphate, efficiently triggered the production. Because the 5′-monophosphate did not enhance the physical association between dsRNA and RIG-I in vitro (Figure 1B and Figure S8), or resultant conformational change, we do not know the mechanism underlying the requirement for the end monophosphate. A transfection experiment (Figure S6) suggested that an end monophosphate may enhance the stability of dsRNA in cytoplasm.

Please cite this article in press as: Takahasi et al., Nonself RNA-Sensing Mechanism of RIG-I Helicase and Activation of Antiviral Immune Responses, Molecular Cell (2008), doi:10.1016/j.molcel.2007.11.028

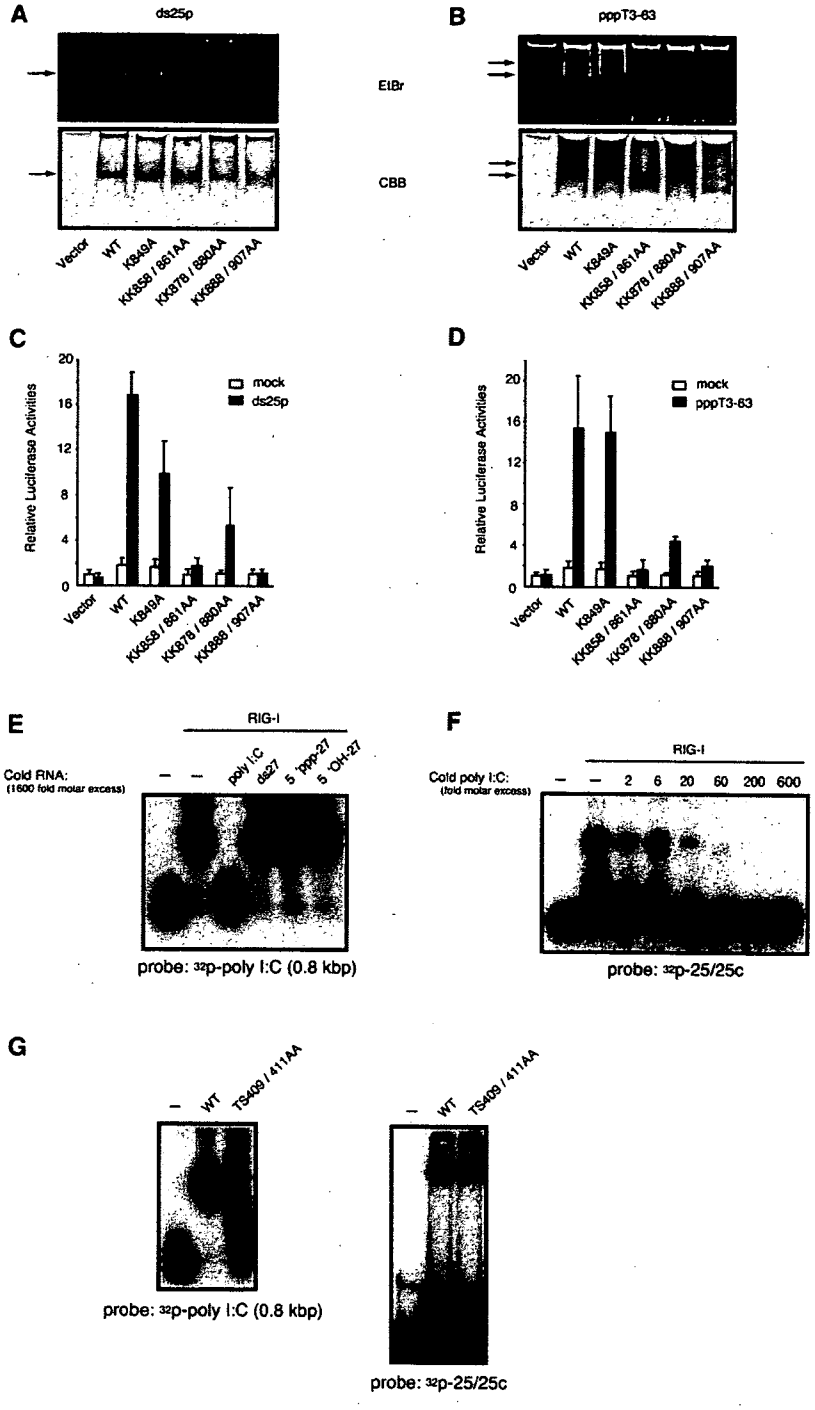

Figure 6. Functional Analysis of the Basic Surface of RIG-I CTD

(A and B) RNA-binding activity of RIG-I and its mutants. Wild-type and indicated mutants were expressed in 293T cells and purified with anti-Flag beads. Proteins were incubated with ds25p (A) or pppT3-63 (B) RNA and subjected to native PAGE. Bound RNA and protein were detected by staining with EtBr (upper panel) and CBB (lower panel), respectively. Although the protein band is smeared, clear RNA-protein complexes were detected (arrows).

(C and D) Activation of wild-type RIG-I and mutants by dsRNA and 5′ppp ssRNA. MEFs derived from *RIG-I*$^{-/-}$ mice were transfected with the reporter gene, p-55C1BLuc, and pRL-tk, together with the expression vector for RIG-I and mutants. Cells were stimulated by transfection with ds25p (C) or pppT3-63 (D) and subjected to a dual-luciferase assay. The values are the means ± SD from triplicate experiments.

(E) EMSA of recombinant RIG-I (10 pmol) using ^{32}P-poly I:C (2.5 fmol) in the absence or presence of indicated cold RNA (each 1600-fold molar excess over probe).

(F) EMSA of recombinant RIG-I (10 pmol) using ^{32}P-25/25c (10 fmol) in the absence or presence of indicated molar excess of cold poly I:C.

(G) Wild-type and TS409/411AA mutant of RIG-I were produced in 293T cells and purified as described in the Experimental Procedures and subjected to EMSA using ^{32}P-poly I:C (left) or ^{32}P-25/25c (right) as probes.

Conformational Change of RIG-I Induced by Binding with Ligand RNA Species

dsRNA and 5′ppp ssRNA recognize overlapping sites on RIG-I and induce similar conformational change, as demonstrated by digestion with trypsin or chymotrypsin. ATP (or AMP-PNP) significantly enhances the conformational change triggered by dsRNA or 5′ppp ssRNA; however, ATP per se is not sufficient to initiate the reaction (Figure 3A). This is consistent with the observation that mutant RIG-I with a disrupted ATP-binding motif (K270A) is incapable of transmitting a signal, although its binding activity to dsRNA and 5′ppp ssRNA is unaffected (Figures 1B and 1C).

CTD as a Nonself RNA Recognition Domain

We found that CTD recognizes both dsRNA and 5′ppp ssRNA. CTD partially overlaps with RD and exhibits activity to bind with the helicase linker region (Figure 3E). Structural analysis by NMR spectroscopy revealed that CTD contains a surface enriched with basic amino acids as well as another surface with acidic patches. NMR titration by dsRNA and 5′ppp ssRNA revealed that these RNAs alter NMR signals derived from the basic surface, including the "basic cleft." Mutagenesis of full-length RIG-I confirmed that the basic surface is critical for the recognition of nonself RNA (Figures 6A–6D). It was surprising to find that a single

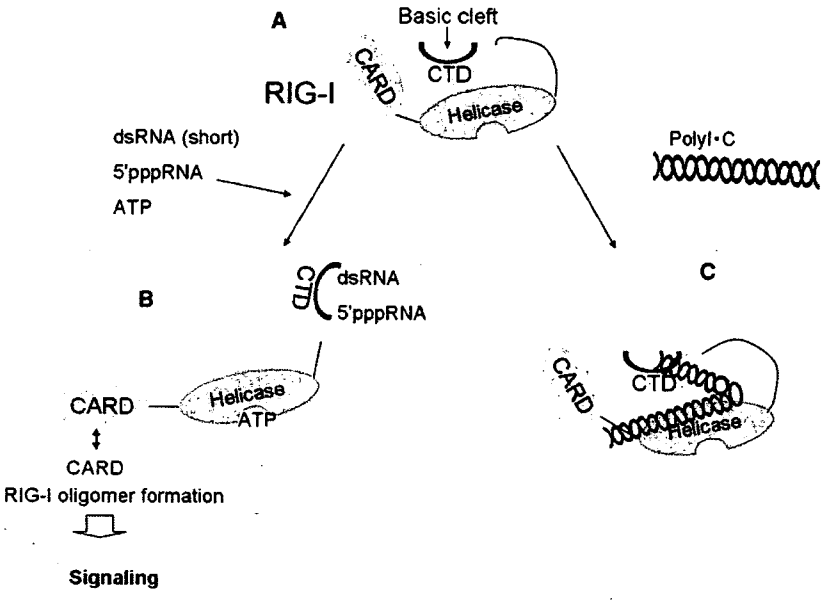

Figure 7. RIG-I Is Activated by Short dsRNA and 5'ppp ssRNA, but Not by poly I:C

(A) Normally RIG-I conforms to closed structure, in which CARD function is repressed, presumably through interaction between CTD and helicase linker region.

(B) When viral infection occurs, short dsRNA or 5'ppp ssRNA is provided to activate RIG-I.

(C) Longer dsRNA such as poly I:C may interact with both CTD and helicase domain of RIG-I. This multipoint interaction allows formation of a stable complex inducing distinct conformation. See text for details.

domain structure is responsible for detecting rather discrete RNA structures. NMR spectra indicate that the loop between β5 and β6, which surrounds the cleft, is flexible (Figure S4), suggesting its involvement in the recognition of different RNA structures and/or conformational change induced by associating with nonself RNA. Interestingly, RIG-I KK878/880AA, which exhibits impaired binding to nonself RNA, is capable of binding with the helicase linker (our unpublished data). Furthermore, none of the mutations on the basic surface are constitutively active (Figures 6C and 6D), suggesting that RD's function may reside on the surface containing acidic patches. This is somewhat reminiscent of 2′-5′-oligoadenylate synthetase, which detects dsRNA by one surface with a basic cleft, and this interaction alters the catalytic domain on the opposite surface (Hartmann et al., 2003).

Analysis of cells derived from *RIG-I*$^{-/-}$ and *MDA5*$^{-/-}$ mice revealed that although poly I:C significantly binds to RIG-I in vitro, it is almost exclusively sensed by MDA5 (Gitlin et al., 2006; Kato et al., 2006). This apparent discrepancy in the binding activity and signaling capability of RIG-I could be partly explained by the observation that poly I:C requires an intact TAS motif in addition to CTD for binding (Figures 6E–6G), thus inducing a conformation distinct from that induced by dsRNA or 5′ppp ssRNA (Figure 3B and Figure S7).

Below is the current model for the activation of RIG-I (Figure 7). RIG-I conforms to a closed structure, in which CARD function is repressed, presumably through the interaction between CTD and the helicase linker region. When viral infection produces short dsRNA or 5′ppp-RNA and is bound to the basic cleft of CTD in the presence of ATP, RIG-I changes its conformation and releases CARD from the constraint. The released CARDs interact with each other to form RIG-I oligomers, relaying a signal through their interaction with IPS-1. When longer dsRNA, such as poly I:C, binds to RIG-I, interaction occurs with the helicase domain as well as with CTD. This multipoint interaction allows the formation of a stable complex, inducing distinct conformation. This complex is abortive, presumably due to its failure to expose CARD.

Poly I:C activates MDA5 in vivo, suggesting that MDA5 and RIG-I are activated differently. CTD of MDA5 is defective in dsRNA binding (Figure S10), and full-length MDA5 binds with poly I:C weakly (Yoneyama et al., 2005). Furthermore, CTD of LGP2 displays a strong binding activity to short dsRNA, but the corresponding region of MDA5 failed to do so. It is worth noting that lysine residue corresponding to K858 of RIG-I, which contributes to nonself RNA recognition (Figure S11), is conserved in LGP2 but is completely missing in MDA5 (Figure 4B). Therefore it is tempting to speculate that MDA5 functions in concert with other factors, such as LGP2.

EXPERIMENTAL PROCEDURES

Oligonucleotides

5′ppp ssRNA was synthesized by in vitro transcription using the T7 Megascript kit (Ambion, Austin, TX). Chemically synthesized RNAs were from Japan Bio Services Co., Ltd. (Saitama, Japan). For generating duplexes, RNA or DNA oligonucleotides were mixed in hybridization buffer (20 mM Tris-HCl [pH 8.0], 1.5 mM $MgCl_2$, and 1.5 mM DTT), boiled for 1 min, and incubated at 37°C for 1 hr. Where indicated, oligonucleotides were 5′ phosphorylated, or dephosphorylation was performed by T4 polynucleotide kinase or alkaline phosphatase (TaKaRa), respectively.

Binding Assay

Recombinant RIG-I proteins were mixed with oligonucleotides in a reaction mixture (10 μl, in hybridization buffer). After incubation at room temperature for 15 min, the reaction mixture was applied to a 7.5% acrylamide gel (Tris-glycin buffer) and stained with EtBr and CBB. When a radioactive probe was used, the mixture was applied to a 15% acrylamide gel (TBE buffer) and the radioactivity was detected with an Image Analyzer (Fuji). ^{32}P-poly I:C was prepared by labeling ~800 bp poly I:C isolated from agarose gel using T4 polynucleotide kinase and [γ-^{32}P]ATP.

Helicase Assay

^{32}P duplexes indicated in Figure S1 were prepared by annealing ^{32}P-25c or ^{32}P-D25c with appropriate complementary cold oligonucleotides. To prevent the reannealing of unwound duplexes, a 1000-fold molar excess of competitor (cold 25-mer oligonucleotide DNA or RNA complementary to ^{32}P-25c) was included in the mixture. The reaction mixture (10 μl), which contains 0.04 pmol ^{32}P-duplex substrate, 40 pmol competitor, 30 pmol recombinant RIG-I protein, 20 mM Tris-HCl (pH 8.0), 1.5 mM $MgCl_2$, 1.5 mM DTT, 70 mM KCl, 5 mM ATP or AMP-PNP, and 2 units/μl RNase Inhibitor (Roche), was incubated at 37°C for 60 min. The mixture was incubated at 37°C for 15 min and applied to a 7.5% SDS gel.

Please cite this article in press as: Takahasi et al., Nonself RNA-Sensing Mechanism of RIG-I Helicase and Activation of Antiviral Immune Responses, Molecular Cell (2008), doi:10.1016/j.molcel.2007.11.028

Plasmids

p-55C1BLuc, pRL-tk, and pEF-flagRIG-I were described previously (Yoneyama et al., 2004). The expression plasmids for RIG-I mutants, pEF-flagRIG-IR849A, pEF-flagRIG-IRK858/861AA, pEF-flagRIG-IRK878/880AA, and pEF-flagRIG-IKK888/907AA, were generated using a GeneEditor in vitro site-directed mutagenesis system (Promega).

Reporter Gene Assay

L929/C1B-Luc cells, stably integrating a reporter construct, p-55C1BLuc, were plated in 48-well plates, and treated with 10^3 units/ml mouse IFN-β for 15 hr and transfected with oligonucleotides using Trans-IT TKO (Invitrogen). After 12 hr, cell extracts were made and subjected to a luciferase assay. RIG-I KO MEFs (5×10^4) were transfected with p-55C1BLuc (0.7 μg), pRL-tk (7 ng), and expression plasmids for RIG-I mutants (1.4 μg) using FuGene6 transfection reagent (Roche). Cells were split into four aliquots, stimulated with RNA transfection for 12 hr, and harvested at 48 hr after DNA transfection.

IRF-3 Dimerization Assay

L929 cells or MEFs were plated in 3 cm dishes, treated with 10^3 units/ml mouse IFN-β for 12 hr, transfected with RNA using Trans-IT TKO, and cultured for 12 hr. Cell extracts were subjected to native PAGE and western blotting (Yoneyama et al., 2004).

Protease Digestion

The binding reaction mixture (10 μl) containing RIG-I (30 pmol) and oligonucleotides (10 pmol) was incubated at room temperature for 15 min. Proteases were added for digestion: trypsin (TPCK-treated trypsin, 0.16 μg, 37°C for 15 min, terminated by TLCK 1 μg/ml) and chymotrypsin (TLCK-treated chymotrypsin, 0.05 μg, 37°C for 30 min, terminated by TPCK 1 μg/ml). One-tenth of the digested RIG-I was analyzed by SDS-PAGE/immunoblotting using anti-human RIG-I monoclonal antibody (clone N3514, epitope: aa 218–792).

Recombinant Proteins

Production and purification of full-length RIG-I (1–925) were described elsewhere (Saito et al., 2007). The CTD (792–925) of human RIG-I was amplified by PCR and inserted into a pGEX-6P-1 vector to produce GST fusion protein (GE Healthcare). Expression vectors were introduced into *Escherichia coli* BL21(DE3) cells and cultured in M9 medium. Protein expression was induced by the addition of 1 mM IPTG when the absorbance at 600 nm was ~0.4. The cells were then grown at 16°C for 24 hr. The protein was purified with glutathione Sepharose 4B (GE Healthcare), then the GST was removed by PreScission protease (GE Healthcare). The protein was further purified with size-exclusion Superdex 75 columns (GE Healthcare). Uniformly labeled protein was expressed as described above, except for using medium containing ^{15}N-ammonium chloride and D-glucose (or 13C-D-glucose), and similarly purified. The NMR sample for structural determination was prepared at 0.5 mM in 50 mM Tris (pH 7), 250 mM NaCl, and 0.5 mM EDTA. The NMR sample for titration was further purified with Resource Q-Sepharose (GE Healthcare) to remove the residual nucleic acid and was prepared at 0.1 mM protein in 50 mM Tris (pH 7), 250 mM NaCl, and 1.5 mM DTT. Ten percent D2O was added to each sample for NMR lock.

293T cells (1×10^6 cells in 6 cm dish) were transfected with 20 μg of expression vector using calcium-phosphate method. At 48 hr after transfection, whole-cell extract was prepared (Yoneyama et al., 2004). The lysate was cleared by centrifugation (75,000 rpm, 10 min) and mixed with anti-Flag bead (Sigma) to adsorb Flag-tagged proteins. The bead was washed extensively, and bound protein was eluted with Flag peptide (Sigma).

For GST fusion proteins, Huh7 or 293T cells (5×10^5 cells in 6 cm dish) were transfected with 2 μg of expression vector using FuGene6 (Roche). At 24 hr after transfection, cell lysate was prepared (Yoneyama et al., 2004). The lysate was adsorbed to glutathione Sepharose 4B, and the GST fusion proteins were eluted with reduced glutathione.

NMR Measurements

NMR spectra were acquired at 15°C on Varian Unity Inova 600 and 800 spectrometers. Data were processed using NMRPipe (Delaglio et al., 1995) and analyzed using Sparky (http://www.cgl.ucsf.edu/home/sparky/). Backbone resonances were assigned using 3D HNCA, HN(CO)CA, HNCACB, CBCA(CO)NH, HNCO, HNCAHA, and HBHA(CO)NH spectra. Side-chain aliphatic atoms were assigned using 3D C(CO)NH, H(CCO)NH, CCH-TOCSY, and HCCH-TOCSY spectra, while aromatic side-chain atoms were assigned using 2D (Hb)Cb(CgCd)Hd, 3D CCH-TOCSY, and 3D HCCH-TOCSY spectra.

Structural Determination

3D ^{15}N-edited NOESY and ^{13}C-edited NOESY spectra (τ_{mix} = 100 ms) were measured to obtain the NOE distance constraints. Backbone ϕ and ψ dihedral angle constraints were generated using the program TALOS (Cornilescu et al., 1999). The structure of RIG-I CTD was determined using CANDID/CYANA 2.1 (Herrmann et al., 2002; Guntert et al., 1997). The best 20 structures were analyzed with PROCHECK-NMR (Laskowski et al., 1996). Structural statistics for RIG-I CTD are shown in Table 1.

NMR Titration

A chemical shift perturbation study of the amide nitrogen and proton signals of RIG-I CTD in ^{1}H-^{15}N HSQC spectra was performed with 5′ppp-GG25, GG25/2+25c, and ssRNAs GG25, 2+25 as control (Figure S1). Aliquots of RNA dissolved in water were added to ^{15}N-labeled RIG-I CTD at 0.1, 0.25, 0.5, 1.0, and 2.0 equivalents.

Supplemental Data

Supplemental Data include Supplemental Experimental Procedures, eleven figures, and one table and can be found with this article online at http://www.molecule.org/cgi/content/full/29/4/■ ■ ■/DC1/.

ACKNOWLEDGMENTS

We thank Dr. M. Horiuchi and Ms. Y. Fujioka for preparing RIG-I CTD. This work was supported by funds from the Ministry of Education, Culture, Sports, Science and Technology of Japan, Japan Society for the Promotion of Science, Nippon Boehringer Ingelheim Co., Ltd., and Mitsubishi Rayon Co., Ltd.

Received: June 18, 2007
Revised: October 1, 2007
Accepted: November 9, 2007
Published online: January 31, 2008

REFERENCES

Akira, S., Uematsu, S., and Takeuchi, O. (2006). Pathogen recognition and innate immunity. Cell *124*, 783–801.

Alexopoulou, L., Holt, A.C., Medzhitov, R., and Flavell, R.A. (2001). Recognition of double-stranded RNA and activation of NF-kappaB by Toll-like receptor 3. Nature *413*, 732–738.

Cordin, O., Banroques, J., Tanner, N.K., and Linder, P. (2006). The DEAD-box protein family of RNA helicases. Gene *367*, 17–37.

Cornilescu, G., Delaglio, F., and Bax, A. (1999). Protein backbone angle restraints from searching a database for chemical shift and sequence homology. J. Biomol. NMR *13*, 289–302.

Delaglio, F., Grzesiek, S., Vuister, G.W., Zhu, G., Pfeifer, J., and Bax, A. (1995). NMRPipe: a multidimensional spectral processing system based on UNIX pipes. J. Biomol. NMR *6*, 277–293.

Fujita, T. (2006). Virology. Sensing viral RNA amid your own. Science *314*, 935–936.

Gitlin, L., Barchet, W., Gilfillan, S., Cella, M., Beutler, B., Flavell, R.A., Diamond, M.S., and Colonna, M. (2006). Essential role of mda-5 in type I IFN responses to polyribonosinic:polyribocytidylic acid and encephalomyocarditis picornavirus. Proc. Natl. Acad. Sci. USA *103*, 8459–8464.

Guntert, P., Mumenthaler, C., and Wuthrich, K. (1997). Torsion angle dynamics for NMR structure calculation with the new program DYANA. J. Mol. Biol. *273*, 283–298.

Hartmann, R., Justesen, J., Sarkar, S.N., Sen, G.C., and Yee, V.C. (2003). Crystal structure of the 2′-specific and double-stranded RNA-activated interferon-induced antiviral protein 2′-5′-oligoadenylate synthetase. Mol. Cell *12*, 1173–1185.

Herrmann, T., Guntert, P., and Wuthrich, K. (2002). Protein NMR structure determination with automated NOE assignment using the new software CANDID and the torsion angle dynamics algorithm DYANA. J. Mol. Biol. *319*, 209–227.

Holm, L., and Sander, C. (1993). Protein structure comparison by alignment of distance matrices. J. Mol. Biol. *233*, 123–138.

Hornung, V., Ellegast, J., Kim, S., Brzozka, K., Jung, A., Kato, H., Poeck, H., Akira, S., Conzelmann, K.K., Schlee, M., et al. (2006). 5′-triphosphate RNA is the ligand for RIG-I. Science *314*, 994–997.

Joklik, W.K. (1991). Interferons. In Fundamental Virology, Second Edition, B.N. Fields and D.M. Knipe, eds. (New York: Raven Press, Ltd.), pp. 343–370.

Kato, H., Sato, S., Yoneyama, M., Yamamoto, M., Uematsu, S., Matsui, K., Tsujimura, T., Takeda, K., Fujita, T., Takeuchi, O., and Akira, S. (2005). Cell type-specific involvement of RIG-I in antiviral response. Immunity *23*, 19–28.

Kato, H., Takeuchi, O., Sato, S., Yoneyama, M., Yamamoto, M., Matsui, K., Uematsu, S., Jung, A., Kawai, T., Ishii, K.J., et al. (2006). Differential roles of MDA5 and RIG-I helicases in the recognition of RNA viruses. Nature *441*, 101–105.

Laskowski, R.A., Rullmann, J.A., MacArthur, M.W., Kaptein, R., and Thornton, J.M. (1996). AQUA and PROCHECK-NMR: programs for checking the quality of protein structures solved by NMR. J. Biomol. NMR *8*, 477–486.

Marques, J.T., Devosse, T., Wang, D., Zamanian-Daryoush, M., Serbinowski, P., Hartmann, R., Fujita, T., Behlke, M.A., and Williams, B.R. (2006). A structural basis for discriminating between self and nonself double-stranded RNAs in mammalian cells. Nat. Biotechnol. *24*, 559–565.

Pause, A., and Sonenberg, N. (1992). Mutational analysis of a DEAD box RNA helicase: the mammalian translation initiation factor eIF-4A. EMBO J. *11*, 2643–2654.

Pichlmair, A., Schulz, O., Tan, C.P., Naslund, T.I., Liljestrom, P., Weber, F., and Reis e Sousa, C. (2006). RIG-I-mediated antiviral responses to single-stranded RNA bearing 5′-phosphates. Science *314*, 997–1001.

Rogers, G.W., Jr., Lima, W.F., and Merrick, W.C. (2001). Further characterization of the helicase activity of eIF4A. Substrate specificity. J. Biol. Chem. *276*, 12598–12608.

Saito, T., Hirai, R., Loo, Y.M., Owen, D., Johnson, C.L., Sinha, S.C., Akira, S., Fujita, T., and Gale, M., Jr. (2007). Regulation of innate antiviral defenses through a shared repressor domain in RIG-I and LGP2. Proc. Natl. Acad. Sci. USA *104*, 582–587.

Samuel, C.E. (2001). Antiviral actions of interferons. Clin. Microbiol. Rev. *14*, 778–809.

Yoneyama, M., and Fujita, T. (2007). Function of RIG-I-like receptors in antiviral innate immunity. J. Biol. Chem. *282*, 15315–15318.

Yoneyama, M., Kikuchi, M., Natsukawa, T., Shinobu, N., Imaizumi, T., Miyagishi, M., Taira, K., Akira, S., and Fujita, T. (2004). The RNA helicase RIG-I has an essential function in double-stranded RNA-induced innate antiviral responses. Nat. Immunol. *5*, 730–737.

Yoneyama, M., Kikuchi, M., Matsumoto, K., Imaizumi, T., Miyagishi, M., Taira, K., Foy, E., Loo, Y.M., Gale, M., Jr., Akira, S., et al. (2005). Shared and unique functions of the DExD/H-box helicases RIG-I, MDA5, and LGP2 in antiviral innate immunity. J. Immunol. *175*, 2851–2858.

Yu, H., and Schreiber, S.L. (1995a). Cloning, Zn2+ binding, and structural characterization of the guanine nucleotide exchange factor human Mss4. Biochemistry *34*, 9103–9110.

Yu, H., and Schreiber, S.L. (1995b). Structure of guanine-nucleotide-exchange factor human Mss4 and identification of its Rab-interacting surface. Nature *376*, 788–791.

Accession Numbers

The coordinates of the 20 lowest energy structures have been deposited in the Protein Data Bank under accession number 2RMJ.

Molecular Cell
Article

The C-Terminal Regulatory Domain Is the RNA 5′-Triphosphate Sensor of RIG-I

Sheng Cui,[1,2,6] Katharina Eisenächer,[4,6] Axel Kirchhofer,[1,2] Krzysztof Brzózka,[1,3] Alfred Lammens,[1,2] Katja Lammens,[1,2] Takashi Fujita,[5] Karl-Klaus Conzelmann,[1,3] Anne Krug,[4] and Karl-Peter Hopfner[1,2,*]
[1]Gene Center
[2]Center for Integrated Protein Science, Department of Chemistry and Biochemistry
[3]Max-von-Pettenkofer Institute
Ludwig-Maximilians-University of Munich, Feodor-Lynen-Strasse 25, 81377 Munich, Germany
[4]Department of Internal Medicine II, Technical University Munich, Ismaninger Strasse 22, 81675 Munich, Germany
[5]Department of Genetics and Molecular Biology, Institute for Virus Research, Kyoto University, Kyoto 606-8507, Japan
[6]These authors contributed equally to this work.
*Correspondence: hopfner@lmb.uni-muenchen.de
DOI 10.1016/j.molcel.2007.10.032

SUMMARY

The ATPase RIG-I senses viral RNAs that contain 5′-triphosphates in the cytoplasm. It initiates a signaling cascade that activates innate immune response by interferon and cytokine production, providing essential antiviral protection for the host. The mode of RNA 5′-triphosphate sensing by RIG-I remains elusive. We show that the C-terminal regulatory domain RD of RIG-I binds viral RNA in a 5′-triphosphate-dependent manner and activates the RIG-I ATPase by RNA-dependent dimerization. The crystal structure of RD reveals a zinc-binding domain that is structurally related to GDP/GTP exchange factors of Rab-like GTPases. The zinc coordination site is essential for RIG-I signaling and is also conserved in MDA5 and LGP2, suggesting related RD domains in all three enzymes. Structure-guided mutagenesis identifies a positively charged groove as likely 5′-triphosphate-binding site of RIG-I. This groove is distinct in MDA5 and LGP2, raising the possibility that RD confers ligand specificity.

INTRODUCTION

The innate immune system is a first line of defense against pathogen infection. The response to pathogens by the innate immune system of mammals is initiated by the detection of pathogen components by host pattern recognition receptors. These receptors specifically recognize molecules such as viral RNA and DNA, pathogen cell wall components, or flagellar proteins (Akira et al., 2006; Hiscott et al., 2006; Meylan et al., 2006). Viral RNA is recognized in the endosome by membrane-bound Toll-like receptors, or in the cytoplasm by retinoic acid inducible gene 1 (RIG-I, also known as DDX58) and melanoma differentiation associated antigen 5 (MDA5, also known as IFIH1 or Helicard) (Kawai and Akira, 2006; Seth et al., 2006). Upon recognition of cytosolic viral RNA, RIG-I and MDA5 bind to the adaptor protein IPS-1 (also known as CARDIF, MAVS, or VISA), which is located in the outer mitochondrial membrane (Kawai et al., 2005; Meylan et al., 2005; Seth et al., 2005; Xu et al., 2005). The interactions of RIG-I or MDA5 with IPS-1 initiate downstream signaling to interferon regulator factor 3 (IRF-3), IRF7, and NF-κB transcription factors, resulting in the antiviral response by interferon production and activation of interferon-stimulated genes as well as NF-κB target genes (Johnson and Gale, 2006).

RIG-I and MDA5 sense different types of viruses (Kato et al., 2006). RIG-I is a sensor for Hepatitis C virus, Sendai virus, influenza virus, vesicular stomatitis virus, rabies virus, and Japanese encephalitis virus, while MDA5 appears to detect only picornaviruses. Recent results show that RIG-I distinguishes viral RNA from the vast amount and variety of cellular RNAs by recognizing 5′-triphosphates, a modification that arises from RNA synthesis by many viruses but is not found on normal capped or processed cellular RNA (Hornung et al., 2006; Pichlmair et al., 2006; Plumet et al., 2007). Because the RIG-I stimulating HCV RNA is not known to contain 5′-pppRNA, nonphosphorylated dsRNA regions could also contribute to RIG-I activation. MDA5 activation can be stimulated by the dsRNA analog polyinosine-polycytidylic acid (poly[I:C]), but the precise determinants of viral RNA detected by MDA5 remain elusive (Gitlin et al., 2006). RIG-I and MDA5 are sequence related to a third protein, laboratory of genetics and physiology 2 (LGP2) (Yoneyama et al., 2005). The function of LGP2 in the innate immune system is less well understood, but it has been observed that expression of LGP2 interferes with the RIG-I-dependent stimulation of interferon production, suggesting it might have a regulatory role (Komuro and Horvath, 2006; Rothenfusser et al., 2005).

RIG-I, MDA5, and LGP2 belong to the superfamily 2 (SF2) helicases or ATPases (Gorbalenya et al., 1988; Hopfner and Michaelis, 2007). These enzymes share seven conserved sequence motifs (referred to as "helicase motifs") that mediate ATP and nucleic acid binding. ATP hydrolysis is typically stimulated by nucleic acid binding and results in a conformational powerstroke. SF2 helicases/ATPases can have diverse mechanistic functions, including separation of nucleic acid duplexes for bona fide helicases, translocation and motor function, or remodeling of nucleic acid structures or protein:nucleic acid complexes. Not all

of them, including RIG-I, MDA5, and LGP2, have been demonstrated to possess helicase activity, and the mechanistic role of ATP binding and hydrolysis to the DECH box domain of RIG-I is unclear.

Among SF2 ATPases, RIG-I, MDA5, and LGP2 possess a unique domain structure. RIG-I and MDA5 consist of two N-terminal caspase activation and recruitment domains (CARDs), a central SF2 type DECH box ATPase domain, and a C-terminal extension of little sequence homology to other proteins. LGP2 lacks the two N-terminal CARDs but contains the DECH box domain, as well as a C-terminal extension. The role of these domains in the function of RIG-I is only partly understood. Overexpression of the tandem CARDs of RIG-I can stimulate interferon production independently of the presence of viral RNA, suggesting that the CARDs mediate IPS-1 activation and downstream signaling (Yoneyama et al., 2004). Mutations in the ATP-binding site or truncation of parts of the DECH box domain abolish RIG-I activity, suggesting that ATP- and nucleic acid substrate-dependent conformational changes are a central part of viral RNA sensing (Hornung et al., 2006; Yoneyama et al., 2004). Recent results have shown that the C-terminal domain is required for RIG-I activity and that overexpression of the C-terminal domain inhibits RIG-I signaling in response to Sendai virus infections (Saito et al., 2007). Based on these findings, current models suggest that viral substrates induce an ATP-dependent conformational change that demasks the N-terminal CARDs for interaction with IPS-1. However, the mode of this activation and the nature of the 5′-triphosphate-binding site have not been revealed.

Here we report structural, biochemical, and in vivo analysis of the C-terminal regulatory domain (RD) of human RIG-I. Remarkably, RD contains a zinc-binding site and is structurally related to GDP/GTP exchange factors of Rab-like small GTPases. The zinc-binding site is essential for RIG-I signaling in vivo and is also conserved in MDA5 and LGP2, suggesting a similar activation principle underlying the function of the three DECH box enzymes. We demonstrate that 5′-triphosphate RNA binding to RD leads to dimerization of RIG-I and stimulation of the ATPase activity. Structure-guided mutagenesis identifies a conserved lysine at the bottom of a positively charged groove as likely recognition motif for RNA 5′-triphosphates. While fold and zinc coordination site are conserved, this lysine and other features of the recognition groove are different in LGP2 and MDA5, suggesting that RD could be a specificity determinant for different viral ligands.

RESULTS AND DISCUSSION

RD Activates and CARDs Inhibit RNA-Stimulated ATPase Activity of RIG-I In Vitro

To reveal domain functions in RNA-stimulated RIG-I activation, we analyzed the in vitro biochemical properties of human RIG-I together with a variety of truncation variants and isolated domains (Figure 1A). In particular, we tested RIG-I fragments that lack the two N-terminal CARDs (denoted "ΔCARD-RIG-I," residues 230–925), lack the C-terminal part that was recently described as repressor domain "RD" (denoted "RIG-I-ΔRD," residues 1–793), or lack both CARDs and RD and comprise the

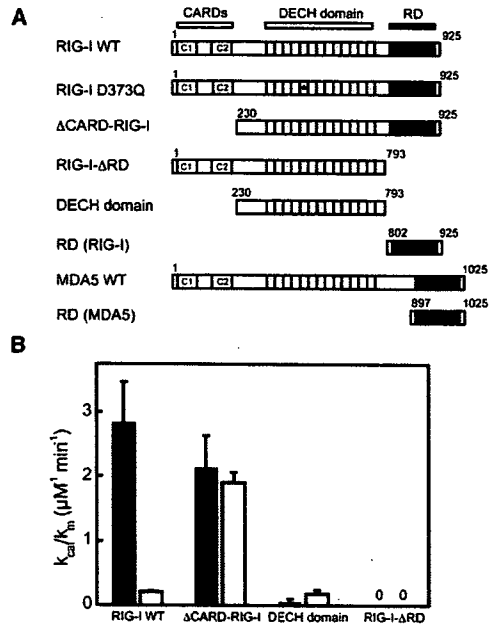

Figure 1. Biochemical Analysis of RIG-I Variants
(A) RIG-I and MDA5 variants used in this study.
(B) Catalytic efficiency (k_{cat} K_m^{-1}) of WT RIG-I and ΔCARD-RIG-I, RIG-I-ΔRD and the DECH domain for pppRVL (black bars), and nonphosphorylated dsRNA (white bars). Error bars represent standard errors of the nonlinear regression analysis (Supplemental Data).

DECH box ATPase domain (denoted "DECH domain," residues 230–793). We identified RD by a combination of limited proteolysis and secondary structure prediction. RD 742–925, similar to the recently published RD domain (Saito et al., 2007), tended to aggregate and was not suited for structural analysis in our hands. With RD 802–925 (denoted as "RD" in the following), we found a stable domain that was suitable for further structural studies.

We tested several RNA molecules for their ability to stimulate the ATPase activity of RIG-I and RIG-I variants in vitro: in vitro-transcribed 5′-triphosphate containing rabies virus leader RNA 58-mer (pppRVL) and 50-mers of nonphosphorylated synthetic ssRNA or dsRNA, corresponding to the sequence of the first 50 bases of RVL. We did not see significant ATPase activity for any RIG-I variants using synthetic ssRNA (see Figure S1 available online). However, pppRVL and synthetic dsRNA had the ability to activate the ATPase activity of RIG-I or some of its variants (Figure 1B). To reveal the efficiency of this activation and the activity of the various RIG-I variants, we measured k_{cat} and K_m values for the ATPase activities and calculated the catalytic efficiencies k_{cat}/K_m (Figure 1B, Figure S2, and Table S1).

We found that WT RIG-I is more efficiently activated by pppRVL than by the same amount of the dsRNA 50-mer. ΔCARD-RIG-I shows an only slightly reduced efficiency for pppRVL than WT RIG-I, indicating that the CARDs are not required for pppRVL stimulation of RIG-I. Remarkably, ΔCARD-RIG-I is much more efficiently stimulated by the nonphosphorylated dsRNA than WT RIG-I, and more or less equally

stimulated by dsRNA as by pppRVL. These results suggest that the CARDs appear to inhibit or block a dsRNA-binding site.

In contrast, a variant that lacks the RD domain was essentially inactive for all types of RNA assayed. This strong effect suggests that RD is required either for RNA binding or that it stimulates the ATPase activity of the DECH box domain by other means. To see whether RD is principally required for the ATPase activity of the DECH domain, we tested the isolated DECH domain for RNA-stimulated ATPase activity. Truncation of the CARDs from RIG-I-ΔRD, forming the isolated DECH domain, rescues some of the ATPase activity, which is now more efficiently stimulated by dsRNA than by pppRVL. This effect suggests that CARDs stabilize an inactive conformation, presumably by blocking an RNA-binding site on the DECH box domain, while RD is required to promote an active conformation of RIG-I in the presence of pppRVL. We do not know whether pppRVL can form local secondary structures or can form transient local duplexes, but the preferential activation of the DECH box domain by dsRNA indicates that in vivo signaling can also involve some sort of dsRNA regions.

The Regulatory Domain of RIG-I Recognizes 5′-Triphosphates

Because ΔCARD-RIG-I still responds to pppRVL and the DECH domain prefers dsRNA, it is unlikely that CARDs or the DECH domain contains the specificity site for RNA 5′-triphosphate recognition. We hypothesized that perhaps RD itself is the RNA 5′-triphosphate sensor of RIG-I. We analyzed the capability of RIG-I and RD to interact with pppRVL using fluorescence anisotropy analysis (Figure 2A). We observed binding isotherms for RIG-I that could be fitted to single site saturation curves. We used fluorescently labeled pppRVL, obtained by including a fluorescent uracil analog (Alexa Fluor 488-5-UTP) in the in vitro transcription reaction. RIG-I binds pppRVL with a K_d of 151 ± 8 nM. Much, but not all, of this binding affinity appears to reside in RD, because RD itself interacts with pppRVL with a K_d = 217 ± 11 nM. To see whether pppRVL recognition by RD depends on the 5′-triphosphate, we repeated the experiments with calf intestine alkaline phosphatase (CIAP)-treated RVL, which is devoid of the 5′-triphosphates. The integrity of the dephosphorylated RNA after CIAP treatment was verified by gel electrophoresis. In contrast to pppRVL, dephosphorylated RVL did not bind with significant affinity to RD. We also did not see significant binding of dsRNA (data not shown). Thus, RD binds to pppRVL in a 5′-triphosphate-dependent manner, suggesting it harbors the RNA 5′-triphosphate-binding site.

It has been previously observed that RD overexpression in cells inhibits RIG-I-dependent signaling in response to Sendai virus infections (Saito et al., 2007). The mechanism of this inhibition remained unclear. If RD binds the 5′-triphosphate, it could inhibit RIG-I by competing for pppRVL. To test this idea, we titrated RD into a solution containing ΔCARD-RIG-I (used because it more or less equally responds to pppRVL and dsRNA) and either pppRVL or nonphosphorylated dsRNA and measured residual ATPase activity. Adding increasing amounts of RD substantially reduced the capability of pppRVL to activate ΔCARD-RIG-I (Figure 2B and Table S2). A dose-dependent inhibition by RD of RIG-I downstream signaling was confirmed by reporter gene experiments in cell culture. Expression of increasing amounts of RIG-I RD domain from transfected plasmids reduced pppRVL-stimulated expression of IFN-β promoter-controlled

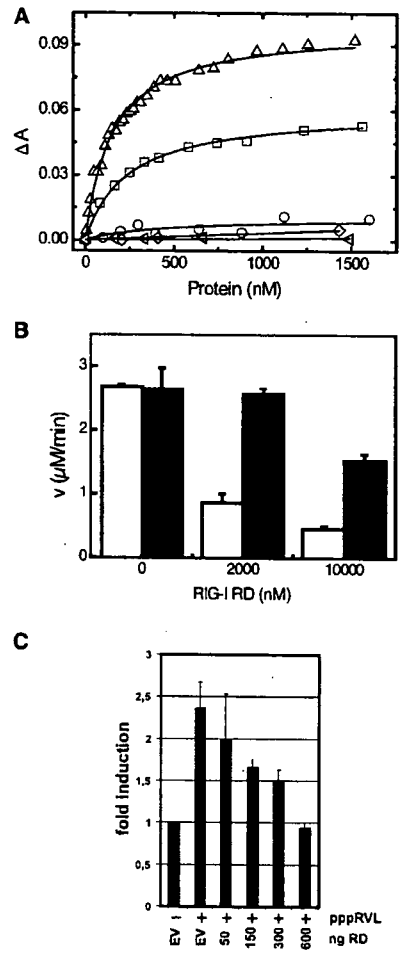

Figure 2. The RIG-I Regulatory Domain RD Binds RNA 5′-Triphosphates

(A) Fluorescence anisotropy changes (ΔA) measured by titrating WT RIG-I (△) or RD (□) into a solution containing fluorescently labeled pppRVL. Nonlinear regression against single site binding isotherms (solid lines) reveals dissociation constants of 151 ± 8 nM for WT RIG-I and 217 ± 11 nM for RD. Titration of RD into dephosphorylated RVL (○) or dsRNA (◁) did not result in significant changes in the anisotropy, suggesting that the 5′-triphosphate confers much of the binding affinity of pppRVL to RD. The RD of MDA5 (◇) also did not result in anisotropy changes for pppRVL.

(B) Dose-dependent inhibition of the ATPase activity of 20 nM ΔCARD-RIG-I by adding indicated amounts of RD in the presence of 200 nM pppRVL (white bars) or 200 nM dsRNA (black bars). Data represent mean and standard deviations (error bars) of three independent measurements.

(C) Dose-dependent inhibition of RIG-I-dependent activation of the IFN-β promoter. 293T cells were transfected with the indicated amounts of plasmids encoding RIG-I-RD or empty plasmid vector (EV) along with 100 ng of WT RIG-I plasmid. Activation of IFN-β promoter-controlled firefly luciferase (p125-FF-Luc) after transfection of 200 ng of pppRVL was determined in the Dual Luciferase Reporter System. Data represent mean and standard deviations (error bars) of three independent measurements.

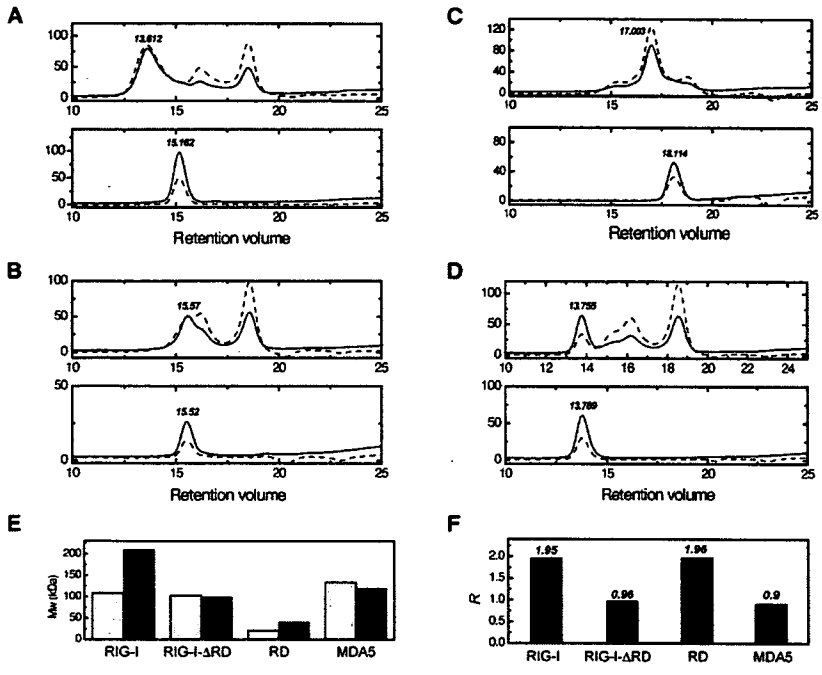

Figure 3. RD Promotes pppRVL-Dependent RIG-I Dimerization

Gel filtration analysis of pppRVL-dependent dimerization of RIG-I (A), RIG-I-ΔRD (B), RD (C), and MDA5 (D) in the presence (upper panels) and absence (lower panels) of pppRVL. Plotted are UV absorption profiles (260 nm, dashed lines; 280 nm, solid lines). The retention volume maxima of the proteins (verified by gel electrophoresis) are indicated. Additional peaks with increased 260 nm over 280 nm absorption stem from free RNA. The molecular weight of the protein fractions was analyzed by light scattering (E) and plotted as relative (*R*) value compared to the calculated monomer weights (F). RIG-I and RD form dimers in the presence of pppRVL while RIG-I-ΔRD and MDA5 are still monomeric, indicating that RIG-I RD promotes specific pppRVL dimer formation of RIG-I.

luciferase assay (Figure 2C). However, we also observe that RD interferes somewhat with the ability of dsRNA to activate ΔCARD-RIG-I, albeit at a much lower level (Figure 2B and Table S2). These effects could be explained if RD has two properties. The much more robust inhibition of pppRVL stimulation than dsRNA stimulation could be explained by competition for pppRVL. The additional weaker inhibition of dsRNA stimulation could be explained if the separately added RD interferes with the activation of the DECH box domain, for instance by interfering with proper multimer formation of RIG-I (see below and Saito et al. [2007]).

pppRVL Binding to RD Dimerizes RIG-I

It has been previously observed that RIG-I activation in cells includes some form of multimer formation that depends on RD (Saito et al., 2007). Thus, we tested whether RD itself is a 5′-triphosphate-dependent multimerization domain and studied the multimerization properties of RIG-I variants along with MDA5 as control by gel filtration and light scattering (Figure 3). In the absence of pppRVL, RIG-I and RIG-I-ΔRD as well as MDA5 are monomeric with apparent molecular weights of 115 kDa, 103 kDa, and 135 kDa. These values match, within the resolution of the experimental method, the expected calculated molecular weights of 109 kDa, 93 kDa, and 118 kDa of monomeric RIG-I, RIG-I-ΔRD, and MDA5. Slightly higher measured molecular weights often indicate nonspherical molecular shapes.

Upon preincubation with pppRVL, RIG-I forms dimers, inferred from apparent molecular weights of 210 kDa. In contrast, MDA and RIG-I-ΔRD still eluted as monomers, with apparent molecular weights of 121 kDa and 99 kDa, indicating that RD of RIG-I is required for pppRVL-dependent dimer formation of RIG-I. This dimer formation is RNA 5′-triphosphate dependent, because synthetic ssRNA 50-mer was unable to induce dimer formation of RIG-I (Figure S3).

We then tested whether RD itself can form dimers and whether this process depends on RNA 5′-triphosphates. In the absence of pppRVL, RD eluted as monomer (21 kDa), while in the presence of pppRVL we observed a molecular weight of 40 kDa. This value is in between the value for an RD dimer (expected MW 34 kDa) and a trimer composed of RD plus one pppRVL (expected MW 53 kDA). One possible explanation for this intermediate value is that the complex transiently dissociates and thus runs at a lower apparent molecular weight. NTPs and nonphosphorylated synthetic ssRNA did not change the elution profile of monomeric RD (Figure S3).

In conjunction with the ATPase and pppRVL binding data (Figures 1 and 2), our results suggest a dual mechanistic role for RD. On one side, it is a recognition domain for RNA 5′-triphosphates; on the other side, it triggers a structural switch that dimerizes RIG-I. Such a dual role also provides an explanation for the observation that RD is not only involved in RIG-I activation by pppRVL but also by dsRNA in vitro (Figure 1B). For instance, if the ATPase activity is stimulated by dimer formation, a lack of dimer formation in RIG-I-ΔRD constructs could reduce ATPase activity for all types of RNA, including dsRNA.

Crystallization and Structural Analysis of RD

To derive a structural framework for this multifunctional role of RD in RIG-I regulation, we crystallized RD and determined the crystal structure to 2.7 Å resolution. We noticed that RD contains several invariant cysteine residues and hypothesized that this region could form a metal-binding site. In fact, our crystals grew in the presence of zinc. To obtain phases, we replaced zinc with mercury by soaking the crystals in a solution that contains Hg-acetate and collected multiple anomalous dispersion data at the mercury L_{III} absorption edge. The resulting electron density allowed us to build all ten RD molecules in the asymmetric unit (Figure 4A and Table 1). We also determined a 3.0 Å crystal

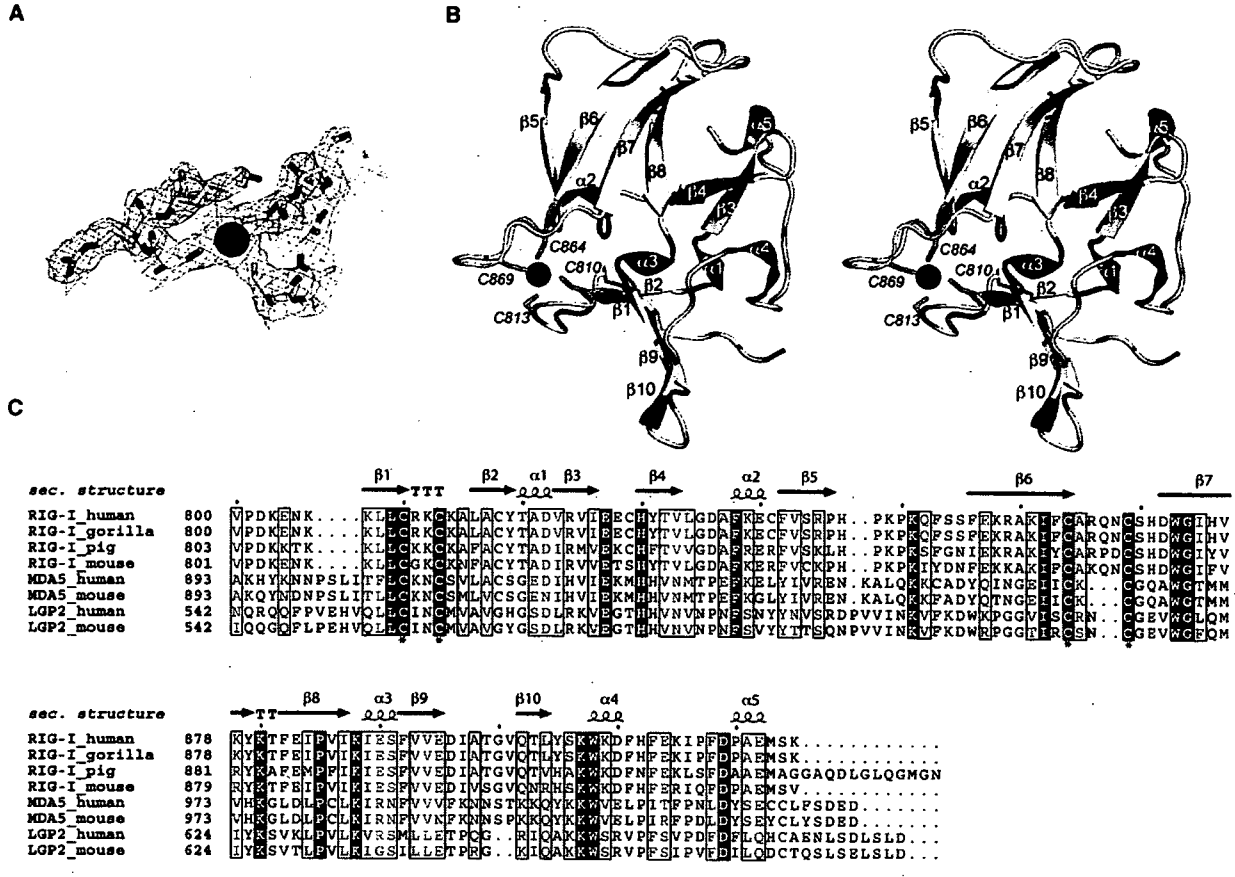

Figure 4. Structure of the Regulatory Domain of Human RIG-I

(A) Portion of the final $2F_o - F_c$ electron density (1 s contour) at the zinc-binding site with superimposed final model.

(B) Stereo image of a ribbon model of RD with highlighted and annotated secondary structure, zinc ion (magenta sphere), and annotated zinc-coordinating cysteines (green sticks).

(C) Structure-based sequence alignment of the C-terminal regions of RIG-I, MDA5, and LGP2 from different species. The secondary structure is shown on top. Invariant residues among RIG-I, LGP2, and MDA5 are highlighted with red background; conserved residues are shown in red font. The zinc-coordinating cysteines are marked with an asterisk.

structure of RD crystallized in the presence of zinc by molecular replacement. Both mercury- and zinc-bound structures, as well as all ten copies in the asymmetric unit, are highly similar to each other.

RD is a flat domain with a concave and convex side and dimensions of 45 Å × 35 Å × 30 Å (Figure 4B). It is structurally organized in three leaves, consisting of two four-stranded (β1, β2, β9, β10, and β5, β6, β7, β8) and one two-stranded (β3, β4) antiparallel β sheets. Small helical turns connect the three β sheets. The two four-stranded β sheets are laterally connected by two protruding loops, each containing two highly conserved cysteine residues (Cys810, Cys813 and Cys864, Cys869). Together, the four thiol groups of these cysteines coordinate the zinc (or mercury) ion in each of the ten molecules in the asymmetric unit (Figures 4A and 4B).

The zinc-coordinating cysteines are invariant not only in all available RIG-I sequences but also in all available MDA5 and LGP2 sequences, suggesting that this motif is a central functional or structural element in the entire family. Sequence representatives are shown in Figure 4C. Apart from the zinc coordination site, several other residues that form the hydrophobic core or are involved in fold stabilization (F838, W873, P885, and W908) are conserved between RIG-I, MDA5, and LGP2. Because these residues are distributed across the RD sequence, the fold of RD is probably conserved between RIG-I, MDA5, and LGP2. One possibility is that RD domains in MDA5 and LGP2 could possess similar, ligand-dependent dimerization functions. We tested whether MDA5 RD can bind to pppRVL (Figure 2A) but did not see significant binding. Thus, either different types of ligands are recognized by "RD" of MDA5, or this domain has a different functional role. For instance, the RD of MDA5 could be involved in detection of RNA elements that resemble poly(I:C), a known activator of MDA5. At present, we could not analyze the RD of LGP2 because of protein instability.

Table 1. Crystallographic Data and Model Statistics

	Hg-Acetate		Native (Zinc)
Data Collection	Inflection	Peak	
Space group	$P2_1$	$P2_1$	$P2_1$
Cell dimensions			
a, b, c (Å)	a = 97.20	a = 97.15	a = 97.9
	b = 76.60	b = 76.54	b = 76.6
	c = 137.80	c = 137.90	c = 139.4
α, β, γ (°)	90, 93.1, 90	90, 93.07, 90	90, 93.3, 90
Wavelength	1.010	1.008	0.9
Resolution (Å)	3.2	2.7	3.0
R_{sym}	7.9 (52.1)[a]	6.7 (43.8)	9.0 (44.5)
I/σI	14.49 (2.58)	14.36 (3.04)	8.97 (2.13)
Completeness (%)	98.3 (94.6)	98.1 (94.4)	98.0 (98.0)
Redundancy	3.87	3.88	2.54
Refinement			
Resolution range (Å)	20–2.7		50–3.0
Number of reflections	48,855		40,897
R_{work}/R_{free}	24.1/27.6		24.8/28.5
Number of atoms			
Protein	9990		9990
Ligand/ion	10 mercury		10 zinc
Water	124		49
B factors			
Protein	51.62		48.66
Rmsd			
Bond lengths (Å)	0.007		0.008
Bond angles (°)	1.49		1.52
PDB accession code	2QFD		2QFB

[a] Highest resolution shell is shown in parentheses.

RIG-I RD Is Structurally Related to MSS4 GDP Exchange Factor of Rab GTPases

Our data from the in vitro ATPase experiments indicate that RD is not only important for 5′-triphosphate binding but also activates the DECH box domain. To learn more about the functional architecture of RD, we looked for structural relatives in the protein data bank (PDB) using the DALI search tool (Holm and Sander, 1993). We found two significant hits (Figure S4). RD is related to the C-terminal methionine sulfoxide reductase domain of PilB (PDB entry 1L1D), although this structure lacks the zinc-binding site. However, both fold and zinc-binding site of RD are related to MSS4, a GDP/GTP exchange factor for small Rab-like GTPases (PDB entry 2FU5) (Figure 5A).

The zinc knuckle protein MSS4 stimulates nucleotide exchange by structurally modulating the nucleotide-binding site of the Rab8 GTPase (Itzen et al., 2006). Hereby, the zinc-binding site and its adjacent β sheets form the main interaction site to Rab8 and are a central element of MSS4-induced local unfolding of Rab8. The capability to locally unfold a GTPase active site is perhaps in part achieved by the rigid, thermodynamically stable architecture of the zinc cluster (Yu and Schreiber, 1995).

The structural similarity in both fold and zinc cluster raises the possibility that RD activates RIG-I not only by binding to 5′-triphosphates and dimer formation but also by some sort of structural modulation of the ATP-binding site, similar to the role of MSS4 in the activation of Rab8. While such a role needs to be addressed in future studies, it predicts that the zinc coordination site is a key functional element of RIG-I activation by RD.

The Zinc-Binding Site Is Essential for RIG-I Function In Vivo

To test the functional relevance of the zinc-coordinating cysteine residues of RD in vivo, we analyzed full-length RIG-I mutants, where RD cysteines have been mutated to arginine (Figure 5C) or alanine (Figure S5). RIG-I RD contains seven cysteines (Figures 4C and 5B). C810, C813, C864, and C869 are conserved in RIG-I, MDA5, and LGP2 and form our identified zinc-binding site. C818, which is conserved between RIG-I and MDA5 but not LGP2, is located close to the zinc-binding site but does not bind the metal ion directly. Two additional cysteine residues (C829 and C841) in the RIG-I RD are conserved between species, but not in MDA5 and LGP2.

Wild-type and mutant RIG-I were tested for their ability to trigger IFN-β promoter activation in response to infection with VSV-M51R (Figure 5C). Overexpression of WT *RIG-I* confers a low level of constitutive IFN-β promoter activation in the absence of ligand (15-fold induction compared to vector control). Infection with VSV-M51R led to a strong induction of IFN-β promoter activity (32-fold compared to mock infected cells expressing WT *RIG-I*). Induction is also observed for *RIG-I* harboring C829R and C841R (nonconserved cysteine) mutations. However, mutation of any one of the four invariant cysteines that coordinated the zinc (C810, C813, C864, and C869) or C818 to arginine abrogated the response to VSV-M51R. These defects, with the exception of C818R, are not due to insufficient protein levels (Figure S6) or to a dominant-negative inhibition of endogenous RIG-I (Figures S5 and S7). Similar results were obtained with mutations of conserved cysteines to alanines (Figure S5) and also in a cell line lacking functional endogenous RIG-I (Huh7.5 [Sumpter et al., 2005]; Figure S5). Activation of the IFN-β promoter after transfection of higher amounts of expression plasmids suggested intact constitutive signaling of RIG-I invariant cysteine mutants (Figure 5C, insert). WT RIG-I was activated by total RNA isolated from VSV-infected cells and by in vitro-transcribed 5′-triphosphate VSV leader RNA (pppVSVL), whereas the RIG-I C→R (mutated in all invariant cysteines of RIG-I RD) did not respond to either of the specific RIG-I ligands tested (Figure 5D). However, similar to WT RIG-I the RIG-I C→R mutant was able to interact with IPS-1 in the absence of RIG-I ligands in cotransfection experiments, confirming integrity of the CARDs in the presence of mutations affecting structure and function of the RD (Figure S8).

Taken together, our data show that the zinc coordination site is a key structural motif of RIG-I in vivo. The strong effect of C818R, which does not coordinate zinc and is located in the hydrophobic core of RD, is likely due to the lack of detectable protein levels, perhaps induced by misfolding (Figure S6). C829 and C841, on the other hand, are located on the RD surface, and the remaining responsiveness of the corresponding mutants to RIG-I ligand argues that these residues are not involved in a critical functional site.

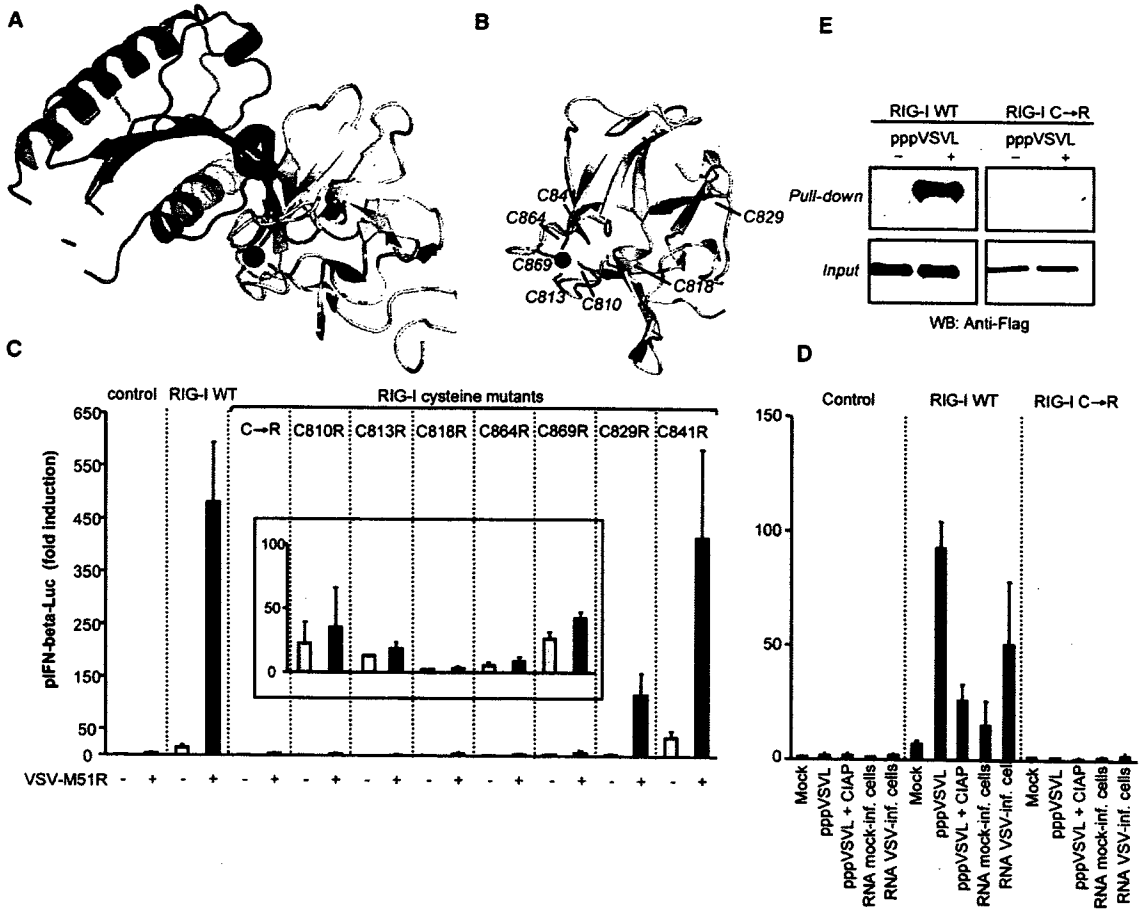

Figure 5. RIG-I Is Related to GDP/GTP Exchange Factors and Contains an Essential Zinc-Binding Site

(A) The fold and zinc-binding site of RD (shown in [B]) are related to GDP/GTP exchange factor MSS4 (yellow/brown ribbon model with green cysteines and magenta zinc). MSS4 induces GDP/GTP exchange in Rab8 (blue ribbon model) by local unfolding (Itzen et al., 2006).

(B) Location of cysteine residues (green sticks) on RD (gray ribbon model with magenta zinc ion).

(C and D) Conserved (C810, C813, C818, C864, C869) and nonconserved (C829, C841) cysteine residues in the RD of RIG-I were mutated to arginine. In the RIG-I C→R mutant, all five conserved cysteines were mutated to arginine. HEK293 cells were transfected with IFN-β promoter luciferase reporter constructs and renilla luciferase control vector as well as plasmids expressing WT RIG-I or RIG-I cysteine mutants using 100 ng or 400 ng per transfection (C, insert). Cells were subsequently stimulated (C) by infection with VSV-M51R and (D) in vitro-transcribed VSV leader RNA (pppVSVL ± dephosphorylation with CIAP) or RNA isolated from mock-infected and VSV-infected HepG2 cells. IFN-β promoter activity was measured by dual luciferase assay after 18 hr (fold induction compared to mock-treated empty vector control). Mean values and standard deviations of five (C) and four (D) independent experiments are shown.

(E) The cytoplasmic fraction of cells transfected with Flag-tagged WT RIG-I or RIG-I C→R mutant was incubated with biotinylated pppVSVL. RNA-protein complexes were pulled down using streptavidin affinity beads. Input and pull-down samples were analyzed by SDS-PAGE and immunoblotting using anti-Flag antibody (one representative of two experiments is shown).

Because RNA 5′-triphosphates appear to directly interact with RD in vitro, we tested whether the integrity of the zinc-binding site disrupts pppVSVL binding of RIG-I in vivo. Cytoplasmic extracts of cells transfected with WT *RIG-I* or the *RIG-I* C→R mutant were incubated with biotinylated pppVSVL and subjected to pull-down assay using streptavidin beads to recover RNA-protein complexes. pppVSVL was found to bind strongly to WT RIG-I, but not to mutant RIG-I (Figure 5E). Therefore, the integrity of the zinc-binding site of RD is essential for binding of pppVSVL by RIG-I in vivo and these data further corroborate our in vitro finding that RD is the RNA 5′-triphosphate sensor of RIG-I.

A Conserved Groove Is Involved in Binding of 5′-pppRVL

Our functional data show that RD does specifically recognize 5′-pppRVL, but not dephosphorylated RVL. Protein sites that bind triphosphates with high affinity, such as the active site of ATPases, often contain a positively charged patch to compensate the negative charge of the triphosphate chain, and the binding sites are often highly sequence conserved. We have not been able to cocrystallize RD with pppRVL or phosphates. To learn more about the potential triphosphate-binding site, we analyzed the sequence conservation and electrostatic potential at the solvent-accessible surface (Figures 6A and 6B). We find a highly

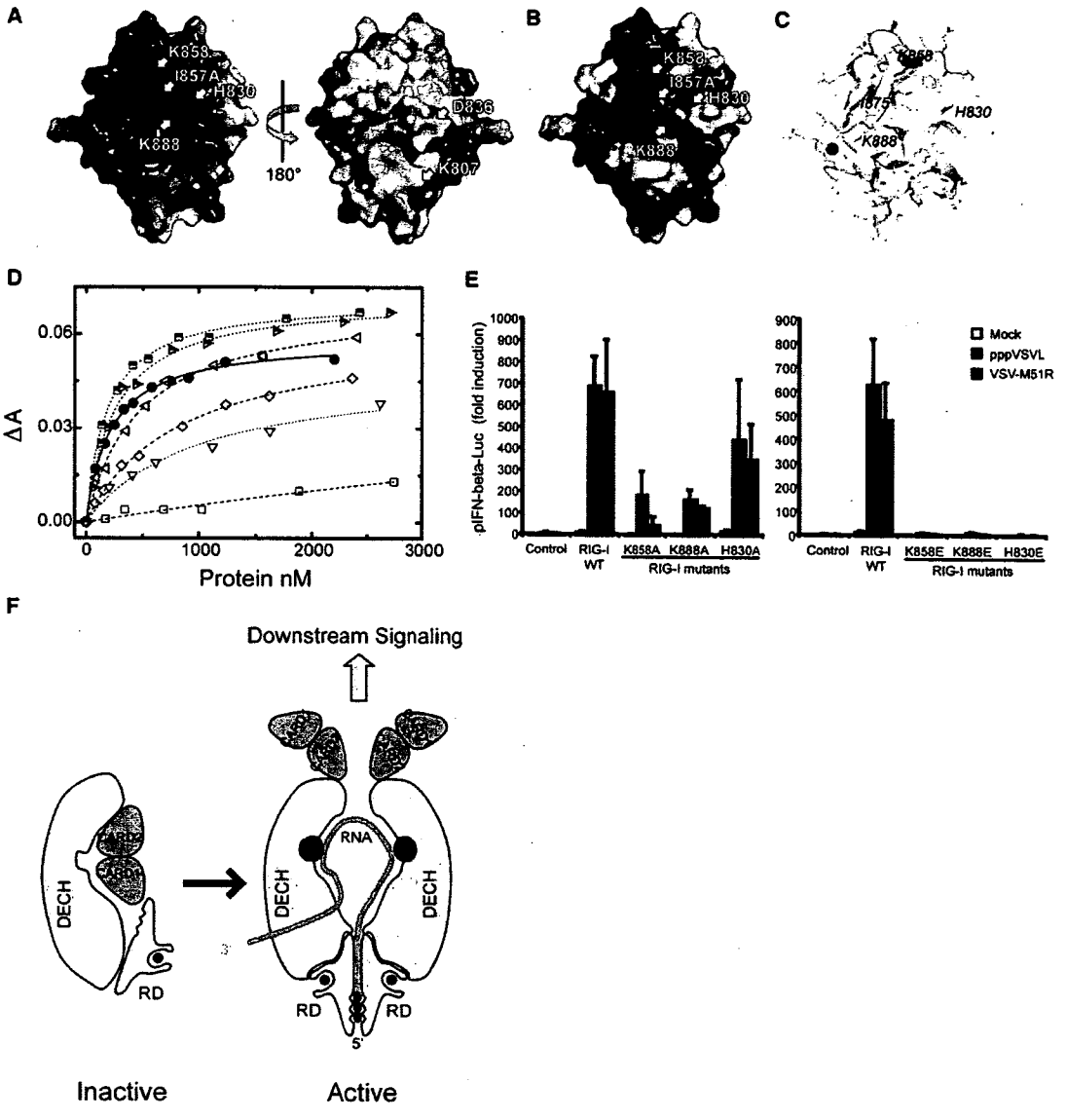

Figure 6. Localization of the RNA 5′-Triphosphate-Binding Site on RD

(A) Electrostatic surface potential (ranging from blue = 9 kT/e to red = −9 kT/e), displayed in two different views (left, "standard view" used in all other figures; right, 180° rotation around vertical axis). The sites of mutated residues are annotated. A prominent positive groove indicates a likely phosphate-binding site for RNA 5′-triphosphates.

(B) Surface conservation of RIG-I RD in standard view, ranging from dark red (invariant) to white (unconserved). A patch of high sequence conservation colocalizes with the positively charged groove (A, left).

(C) Localization of the mutations, shown in a ribbon model with added side chains. The effect of alanine mutations on pppRVL binding in vitro is highlighted by different colors: red, large effect; orange, medium effect.

(D) Fluorescence anisotropy changes (ΔA) of fluorescently labeled pppRVL in response to titration with WT RD (filled circle, K_d = 217 ± 11 nM) and mutated RD using the setup of Figure 2A. Two control mutations of conserved residues of the convex side of RD, K807→A (half-filled right-facing triangle, K_d = 254 ± 16 nM) and D836→A (half-filled square, K_d = 185 ± 15 nM), did not significantly alter binding affinity of pppRVL. Several mutations in the positively charged groove reduced binding affinity. H830→A (open left-facing triangle, K_d = 500 ± 30 nM); I875→A (open diamond, K_d = 1.0 ± 0.1 μM), and K888→A (open down-facing triangle, K_d = 1.0 ± 0.2 μM) significantly reduced binding affinity. K858→A (open square, K_d > 5 μM), however, dramatically reduced binding affinity, indicating that this residue is a central recognition site for pppRVL.

(E) HEK293 cells were transfected with IFN-β promoter luciferase reporter constructs and renilla luciferase control vector as well as plasmids expressing WT RIG-I or indicated mutants (10 and 100 ng per transfection). The left panel depicts the more conservative alanine mutants, while the right panel depicts the stronger glutamate charge reversal mutants. Cells were stimulated with transfected pppVSVL or infected with VSV-M51R. IFN-β promoter activity was measured by dual

positively charged groove at the concave side of RD that colocalizes with a region of high sequence conservation. To analyze this putative RNA 5′-triphosphate recognition site, we tested a variety of RD mutants in this region for interaction with pppRVL, using our fluorescence anisotropy assay (Figures 6C and 6D and Table S3).

Two control mutations (K807A and D836A), located on the convex side of RD, did not significantly alter the binding affinity for pppRVL, although these residues are highly sequence conserved. In contrast, three mutations in conserved residues inside the positively charged groove significantly reduced the binding affinity (H830A, I875A, and K888A). The mutation K858A, however, located at the center of the positive patch, dramatically reduced binding of pppRVL. This strong effect indicates that the groove is involved in the binding of the RNA 5′-triphosphate. We tested the K858A, K888A, and H830A mutants in vivo and found a significant reduction, but not complete abrogation of IFN-β promoter activity induced by transfection with pppVSVL or infection with VSV-M51R (Figure 6E, left). Mutations to negatively charged glutamates in the same positions (K858E, K888E, and H830E) entirely abrogated the response to pppVSVL and VSV-M51R (Figure 6E, right). The similar relative reductions in activity of the mutants in in vitro and in vivo experiments argue that the RNA binding defects observed in vitro are also the cause of reduced activity in vivo. Together, these observations suggest that interaction of VSV-RNA with the positively charged patch of the groove is required for full activation of RIG-I in vivo.

We do not see significant binding of fluorescently labeled UTP to RD (data not shown), which also contains a triphosphate. Thus, RD recognizes more than the triphosphate and sugar/base moiety of the 5′-terminal base of pppRNA. However, if RNA extends from K858 along the longest dimension of RD, the footprint will cover at most three bases, indicating that recognition of viral RNA by RD is limited to the very 5′-terminal region. This argues that adjacent 3′ regions could then bind to the RNA-binding sites of the DECH box domain.

Proposed Model for RD-Dependent RIG-I Activation

In summary, our data suggest a model for RIG-I activation that includes the following chain of events (Figure 6F). In the absence of 5′-triphosphate containing RNA ligands, RIG-I is monomeric and inactive. The CARDs probably partially mask an RNA-binding site on the DECH box domain. The preference of the DECH domain for dsRNA indicates that this RNA-binding site could also recognize secondary structures of virus RNA. pppRNA binding to RD induces a conformational change in the enzyme that results in dimerization and stimulation of the DECH box domain. The dimer form could, for instance, enable the binding of dsRNA or other types of RNA to the DECH domain by displacing the CARDs, and, in conjunction with or coupled to RNA-stimulated ATPase activity, this structural change might generate a signaling conformation of RIG-I. In analogy to adenosine triphosphate binding-dependent structural switches in many ATPases (Hopfner and Tainer, 2003), the binding energy of RNA 5′-triphosphates, which is likely in the same range as the binding energy of ATP to ATPases, is well suited to trigger such a macromolecular conformational change.

RIG-I RD mutants that have strongly reduced signaling activity are still able to interact with IPS-1 (Figure S8). We do not know at the moment how a RIG-I:IPS-1 interaction might lead to initiation of downstream signaling. Our dimerization results make it likely that the IPS-1:RIG-I signaling conformation includes a RIG-I dimer and for that reason possibly also an IPS-1 dimer. Because RD helps to stabilize an inactive conformation of CARDs (Saito et al., 2007), RD mutations might allow or even stimulate CARD exposure and thus IPS-1 interaction, but prevent pppRVL-induced RIG-I dimer formation and for that reason signal induction.

In conclusion, our data reveal the binding site for 5′-triphosphates on RIG-I, located on the C-terminal regulatory RD domain. At the center of this binding site is a RIG-I invariant lysine residue that is critically required for triphosphate binding. This lysine is partially buried, similar to the lysine in the P loop of NTPase, and this location is well suited for phosphate interaction. Interestingly, LGP2 contains a proline at the position of RIG-I K858, while MDA5 either contains a threonine or an isoleucine (Figure 4C). Consistent with this observation, we did not see strong binding of pppRVL to RDs of MDA5 and LGP2 (data not shown). Thus, RDs of MDA5 or LGP2 might either bind to different types of ligands or fulfill different functional roles. In any case, the RD of the three related DECH box ATPases could be an important specificity element. Thus, our results not only provide a structural framework to further analyze the specific recognition of viral RNA synthesis products by RIG-I, but could also to help to reveal the recognition of any ligands by the RDs of MDA5 or LGP2.

EXPERIMENTAL PROCEDURES

Protein Expression and Purification

RIG-I and MDA5 were expressed in insect cells as described previously (Berger et al., 2004). Briefly, cDNA was cloned into pFBDM vectors (MultiBac system, kindly provided by I. Berger) and transformed into DH10MultiBac cells. The bacmids were extracted for transfection into High-five insect cells (Invitrogen). Seventy-two hours after infection, the cells were harvested and lysed by "freeze and thaw." All other RIG-I and MDA5 constructs were expressed in *E. coli* BL21 Rosetta cells (Novagen), using pET expression vectors (Novagen). Cultures were grown at 37°C to an OD_{600} of 0.8. Expression was induced by addition of 0.5 mM IPTG, and cells were subsequently incubated at 18°C overnight, with shaking. After harvesting, resuspended cells were disrupted by sonication. All recombinant proteins were purified to homogeneity using metal affinity (QIAGEN) or Strep-Tactin fast flow (IBA), ion exchange, and gel filtration chromatography with standard protocols (GE Healthcare).

ATPase Assays

ATPase assay reaction mixtures (50 μl) contained 20 mM Tris-HCl (pH 7.5), 8 mM DTT, 5 mM $MgCl_2$, 10 mM KCl, 4% (w/v) glycerol, 80 μg/ml BSA, and the specified RNA (10 ng/μl) plus a trace amount of [γ-^{32}P]ATP (2 nM) mixed with different amounts of nonradioactive ATP and 20 nM enzyme. The

luciferase assay after 18 hr (fold induction compared to mock-treated empty vector control). Mean values and standard deviations (error bars) of three independent experiments are shown.

(F) Proposed model for RNA 5′-triphosphate (gray with red phosphates) activation of RIG-I by ligand-induced dimer formation of RD (yellow with magenta zinc ion). RNA stoichiometry and domain-domain interactions are tentative.

reactions were initiated by the addition of enzyme and incubated at 37°C. Samples (1 μl) were removed at 3 min intervals and evaluated by thin-layer chromatography. k_{cat} and V_{max} values were calculated by nonlinear curve fitting of multiple (two to five) independent determinations (see Table S2).

Molecular Weight Determination by Size-Exclusion Chromatography and Light Scattering

Assays were done on a GE Äcta system equipped with a Superose 6 10/300 (GE Healthcare) gel filtration column and connected to a Viscotek VE 3580 RI detector and Viscotek 270 DUAL detector. The gel filtration buffer was 30 mM Tris-HCl (pH 7.5), 150 mM NaCl, 2 mM DTT, and 10 μM $ZnCl_2$. UV absorption, refractive index, and low angle light scattering signals were collected. The system was calibrated with BSA (MW 67,000 Da) standard solution with a concentration of 2 mg/ml.

Fluorescence and Anisotropy Measurement

Fluorescence anisotropy experiments were performed with a FluoroMax-P fluorimeter (HORIBA Jobin Yvon), equipped with a Glan-Thompson prism polarizer. Typically, 1.2 ml of buffer (30 mM Tris-HCl [pH 7.5], 150 mM NaCl, 2 mM DTT, and 10 μM $ZnCl_2$) and 50 nM RNA (in vitro-transcribed pppRVL with incorporated Alexa Fluor 488-5-UTP) were pre-equilibrated in a quartz cuvette at 12°C. Protein samples were added in a stepwise manner and briefly mixed by magnetic stirring. After 3 min re-equilibration, the anisotropy data were collected using an excitation wavelength of 492 nm and monitoring the emission 516 nm. The band pass was 5 nm for excitation and 5 nm for emission. A maximum number of ten trials were performed until less than 2% deviation of the signal was reached.

In Vivo RD Titration Experiments

Reporter gene assays for activation of IFN-β promoter were performed in HEK293T cells seeded in 24-well plates. At a confluence of 75%, cells were transfected with 100 ng IFN-β firefly reporter plasmid (p125luc) and 1 ng of a plasmid encoding CMV-controlled renilla luciferase (pRL-CMV, Promega) as a control, using Lipofectamine 2000 (Invitrogen). In addition, cells were transfected with 100 ng of pEF-BOS-RIG-I full-length plasmid and the indicated increasing amounts of pCAGGS-RIG-I RD expression construct. Twenty-four hours after DNA transfection, cells were transfected with 200 ng in vitro-transcribed pppRVL to stimulate IFN production. Cells were lysed after 24 hr incubation and analyzed for dual reporter gene activity according to the supplier's instructions (Promega) in a Luminometer (Berthold).

In Vivo Analysis of RIG-I Mutants

HEK293 cells (DSMZ, Braunschweig, Germany) were maintained in DMEM with supplements (0.6 g/l L-Glu, 10% FBS, and 1% Pen/Strep from GIBCO-Invitrogen, Karlsruhe, Germany). BHK21 cells (ATCC) were grown in Glasgow medium supplemented with 0.6 g/l L-Glu, 10% FBS, 1% Pen/Strep, and 1% tryptose broth (GIBCO-Invitrogen). Cell cultures were incubated at 37°C with 5% CO_2. VSV-M51R mutant was kindly provided by O. Ebert (TU Munich). Virus stock and plaque assay on BHK21 cells have been described. Mutants of Flag-RIG-I (kindly provided by T. Fujita) were generated using the QuikChange Site-Directed Mutagenesis Kit (Stratagene, Amsterdam, Netherlands) and sequenced. HEK293 cells (2×10^5 cells/24-well) were transiently transfected with 10 ng of pRL-TK reporter (renilla luciferase under control of TK promoter, Promega, Mannheim, Germany), 100 ng of pIFN-β-Luc (firefly luciferase under control of mIFN-β promoter, kindly provided by T. Taniguchi), and 10, 100, or 400 ng of RIG-I constructs or empty control vector using Lipofectamine 2000 (Invitrogen, Karlsruhe, Germany). Eighteen hours after transfection, cells were either infected with 10 moi VSV-M51R or transfected with 1 μg/ml in vitro-transcribed pppVSVL or RNA isolated from mock-infected and VSV-infected cells using Lipofectamine 2000. Cell extracts were prepared and assayed in the Dual Luciferase Reporter System (Promega) after 18 hr.

RNA Pull-Down Experiments

5′-triphosphate RNA encompassing the VSV leader RNA sequence (pppVSVL) was generated by in vitro transcription from a template DNA generated by PCR using plasmid rVSV-EGFP (kindly provided by O. Ebert) as template and 5′ T7 primer (MAXIscript T7 Kit, Ambion, Huntingdon, UK). The DNA template was removed by DNase I treatment, and RNA was purified using Nuc Away Columns (Ambion). For removal of 5′-triphosphates, 20 μg of RNA was treated with 30 U CIAP (NEB, Frankfurt/Main, Germany) for 2 hr at 37°C in the presence of RNase inhibitor (Fermentas, St. Leon, Germany) and extracted with phenol-chloroform. Biotinylated pppVSVL was transcribed from the template DNA described above by using the AmpliScribe Flash T7 Kit (Epicenter, Madison, USA) and biotin-16-uridine-5′-triphosphate (Roche, Mannheim, Germany). RNA binding assays were performed as described (Saito et al., 2007): cytoplasmic extracts were prepared from 3×10^8 HEK293 cells transfected with Flag-RIG-I plasmids. The extracts were incubated with biotinylated pppVSVL and subjected to pull-down with streptavidin agarose beads (Sigma-Aldrich, Munich, Germany), followed by SDS-PAGE analysis and immunoblotting with anti-Flag M2 antibody (Sigma-Aldrich, Munich, Germany).

Crystallization and Structure Determination

RD was crystallized by mixing 2 μl protein (20 mg ml^{-1} in 30 mM Tris-HCl [pH 7.5], 150 mM NaCl, 2 mM DTT, and 10 μM $ZnCl_2$) with 2 μl buffer containing 0.1 M CHES (pH 10.0) and 18% w/v PEG 8000 in a sitting drop vapor diffusion system at 20°C. The derivative used for phase determination was prepared by soaking the crystals for 10 min in 2 mM mercury acetate, 0.1 M CHES (pH 10.0), and 18% w/v PEG 8000. Cryocooling was achieved by soaking the crystals for 5–10 s in reservoir solution containing 15% D(-)-2,3-butanediol and flash-freezing in liquid nitrogen. Highly redundant multiwavelength anomalous dispersion (MAD) data to 2.7 Å on mercury-containing and to 3 Å on native crystals were collected at beamlines PX SLS (Villigen, Switzerland) and ID23-2, ESRF (Grenoble, France). The data sets were processed with XDS (Kabsch, 1993). The space group was identified as P21, and 10 molecules were found per asymmetric unit. One mercury atom was located per molecule and initial phases were calculated and refined with the program AUTOSHARP (Global Phasing, Cambridge), leading to an interpretable electron density map. The manual model building was carried out by using the program Coot (Emsley and Cowtan, 2004). Prior to model building and refinement, we randomly omitted 10% of the reflections for monitoring the free R value. Refinement was performed with CNS V.1.1 (Brunger et al., 1998) and included overall anisotropic B factor and bulk solvent corrections, individual B factor refinement, simulated annealing, and positional refinement. Initial NCS restraints were gradually removed in the final cycles of the refinement, to allow some structural variations. Data collection and model statistics are summarized in Table 1. Figures were prepared with PyMOL (DeLano Scientific).

Supplemental Data

Supplemental Data include eight figures and three tables and can be found with this article online at http://www.molecule.org/cgi/content/full/29/2/169/DC1/.

ACKNOWLEDGMENTS

We thank Wolfgang Reindl for experimental help and Imre Berger for help with the MultiBac expression system. We thank the staffs of PXI (Swiss Light Source, Villingen) and ID14 (European Synchrotron Radiation Facility, Grenoble) for beam time allowance and help with data collection. This work was supported by the German Research Council DFG Sonderforschungsbereich 455 to K.-P.H., A. Krug, and K.-K.C. and by the Center for Integrated Protein Science and Munich Center for Advanced Photonics to K.-P.H. A. Kirchhofer acknowledges support by the DFG Graduate School 1202. This work is part of the theses of K.E. and A. Kirchhofer.

Received: April 6, 2007
Revised: July 12, 2007
Accepted: October 24, 2007
Published: January 31, 2008

REFERENCES

Akira, S., Uematsu, S., and Takeuchi, O. (2006). Pathogen recognition and innate immunity. Cell *124*, 783–801.

Berger, I., Fitzgerald, D.J., and Richmond, T.J. (2004). Baculovirus expression system for heterologous multiprotein complexes. Nat. Biotechnol. *22*, 1583–1587.

Brunger, A.T., Adams, P.D., Clore, G.M., DeLano, W.L., Gros, P., Grosse-Kunstleve, R.W., Jiang, J.S., Kuszewski, J., Nilges, M., Pannu, N.S., et al. (1998). Crystallography & NMR system: a new software suite for macromolecular structure determination. Acta Crystallogr. D Biol. Crystallogr. *54*, 905–921.

Emsley, P., and Cowtan, K. (2004). Coot: model-building tools for molecular graphics. Acta Crystallogr. D Biol. Crystallogr. *60*, 2126–2132.

Gitlin, L., Barchet, W., Gilfillan, S., Cella, M., Beutler, B., Flavell, R.A., Diamond, M.S., and Colonna, M. (2006). Essential role of mda-5 in type I IFN responses to polyriboinosinic:polyribocytidylic acid and encephalomyocarditis picornavirus. Proc. Natl. Acad. Sci. USA *103*, 8459–8464.

Gorbalenya, A.E., Koonin, E.V., Donchenko, A.P., and Blinov, V.M. (1988). A novel superfamily of nucleoside triphosphate-binding motif containing proteins which are probably involved in duplex unwinding in DNA and RNA replication and recombination. FEBS Lett. *235*, 16–24.

Hiscott, J., Lin, R., Nakhaei, P., and Paz, S. (2006). MasterCARD: a priceless link to innate immunity. Trends Mol. Med. *12*, 53–56.

Holm, L., and Sander, C. (1993). Protein structure comparison by alignment of distance matrices. J. Mol. Biol. *233*, 123–138.

Hopfner, K.P., and Tainer, J.A. (2003). Rad50/SMC proteins and ABC transporters: unifying concepts from high-resolution structures. Curr. Opin. Struct. Biol. *13*, 249–255.

Hopfner, K.P., and Michaelis, J. (2007). Mechanisms of nucleic acid translocases: lessons from structural biology and single-molecule biophysics. Curr. Opin. Struct. Biol. *17*, 87–95.

Hornung, V., Ellegast, J., Kim, S., Brzozka, K., Jung, A., Kato, H., Poeck, H., Akira, S., Conzelmann, K.K., Schlee, M., et al. (2006). 5′-triphosphate RNA is the ligand for RIG-I. Science *314*, 994–997.

Itzen, A., Pylypenko, O., Goody, R.S., Alexandrov, K., and Rak, A. (2006). Nucleotide exchange via local protein unfolding—structure of Rab8 in complex with MSS4. EMBO J. *25*, 1445–1455.

Johnson, C.L., and Gale, M., Jr. (2006). CARD games between virus and host get a new player. Trends Immunol. *27*, 1–4.

Kabsch, W. (1993). Automatic processing of rotation diffraction data from crystals of initially unknown symmetry and cell constants. J. Appl. Crystallogr. *21*, 916–924.

Kato, H., Takeuchi, O., Sato, S., Yoneyama, M., Yamamoto, M., Matsui, K., Uematsu, S., Jung, A., Kawai, T., Ishii, K.J., et al. (2006). Differential roles of MDA5 and RIG-I helicases in the recognition of RNA viruses. Nature *441*, 101–105.

Kawai, T., and Akira, S. (2006). Innate immune recognition of viral infection. Nat. Immunol. *7*, 131–137.

Kawai, T., Takahashi, K., Sato, S., Coban, C., Kumar, H., Kato, H., Ishii, K.J., Takeuchi, O., and Akira, S. (2005). IPS-1, an adaptor triggering RIG-I- and Mda5-mediated type I interferon induction. Nat. Immunol. *6*, 981–988.

Komuro, A., and Horvath, C.M. (2006). RNA- and virus-independent inhibition of antiviral signaling by RNA helicase LGP2. J. Virol. *80*, 12332–12342.

Meylan, E., Curran, J., Hofmann, K., Moradpour, D., Binder, M., Bartenschlager, R., and Tschopp, J. (2005). Cardif is an adaptor protein in the RIG-I antiviral pathway and is targeted by hepatitis C virus. Nature *437*, 1167–1172.

Meylan, E., Tschopp, J., and Karin, M. (2006). Intracellular pattern recognition receptors in the host response. Nature *442*, 39–44.

Pichlmair, A., Schulz, O., Tan, C.P., Naslund, T.I., Liljestrom, P., Weber, F., and Reis e Sousa, C. (2006). RIG-I-mediated antiviral responses to single-stranded RNA bearing 5′-phosphates. Science *314*, 997–1001.

Plumet, S., Herschke, F., Bourhis, J.M., Valentin, H., Longhi, S., and Gerlier, D. (2007). Cytosolic 5′-triphosphate ended viral leader transcript of measles virus as activator of the RIG I-mediated interferon response. PLoS ONE *2*, e279. 10.1371/journal.pone.0000279.

Rothenfusser, S., Goutagny, N., DiPerna, G., Gong, M., Monks, B.G., Schoenemeyer, A., Yamamoto, M., Akira, S., and Fitzgerald, K.A. (2005). The RNA helicase Lgp2 inhibits TLR-independent sensing of viral replication by retinoic acid-inducible gene-I. J. Immunol. *175*, 5260–5268.

Saito, T., Hirai, R., Loo, Y.M., Owen, D., Johnson, C.L., Sinha, S.C., Akira, S., Fujita, T., and Gale, M., Jr. (2007). Regulation of innate antiviral defenses through a shared repressor domain in RIG-I and LGP2. Proc. Natl. Acad. Sci. USA *104*, 582–587.

Seth, R.B., Sun, L., Ea, C.K., and Chen, Z.J. (2005). Identification and characterization of MAVS, a mitochondrial antiviral signaling protein that activates NF-kappaB and IRF 3. Cell *122*, 669–682.

Seth, R.B., Sun, L., and Chen, Z.J. (2006). Antiviral innate immunity pathways. Cell Res. *16*, 141–147.

Sumpter, R., Jr., Loo, Y.M., Foy, E., Li, K., Yoneyama, M., Fujita, T., Lemon, S.M., and Gale, M., Jr. (2005). Regulating intracellular antiviral defense and permissiveness to hepatitis C virus RNA replication through a cellular RNA helicase, RIG-I. J. Virol. *79*, 2689–2699.

Xu, L.G., Wang, Y.Y., Han, K.J., Li, L.Y., Zhai, Z., and Shu, H.B. (2005). VISA is an adapter protein required for virus-triggered IFN-beta signaling. Mol. Cell *19*, 727–740.

Yoneyama, M., Kikuchi, M., Natsukawa, T., Shinobu, N., Imaizumi, T., Miyagishi, M., Taira, K., Akira, S., and Fujita, T. (2004). The RNA helicase RIG-I has an essential function in double-stranded RNA-induced innate antiviral responses. Nat. Immunol. *5*, 730–737.

Yoneyama, M., Kikuchi, M., Matsumoto, K., Imaizumi, T., Miyagishi, M., Taira, K., Foy, E., Loo, Y.M., Gale, M., Jr., Akira, S., et al. (2005). Shared and unique functions of the DExD/H-box helicases RIG-I, MDA5, and LGP2 in antiviral innate immunity. J. Immunol. *175*, 2851–2858.

Yu, H., and Schreiber, S.L. (1995). Structure of guanine-nucleotide-exchange factor human Mss4 and identification of its Rab-interacting surface. Nature *376*, 788–791.

Accession Numbers

The Protein Data Bank (PDB) accession number for coordinates and structure factors of zinc-bound RD is 2QFB. The PDB accession number for coordinates and structure factors of mercury-bound RD is 2QFD.

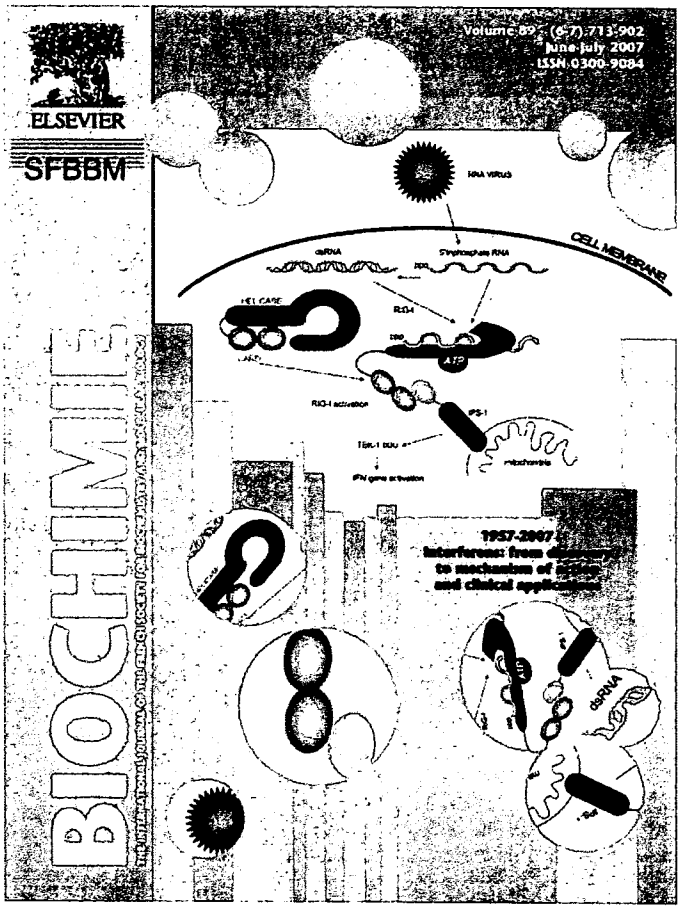

Available online at www.sciencedirect.com
ScienceDirect
Biochimie 89 (2007) 754–760
BIOCHIMIE
www.elsevier.com/locate/biochi

Triggering antiviral response by RIG-I-related RNA helicases

Takashi Fujita*, Kazuhide Onoguchi, Koji Onomoto, Reiko Hirai, Mitsutoshi Yoneyama

Laboratory of Molecular Genetics, Institute for Virus Research, Kyoto University, Kyoto 606-8507, Japan

Received 21 December 2006; accepted 29 January 2007
Available online 20 February 2007

Abstract

TLRs detect several classes of virus-associated molecules, such as ssRNA, CpG-DNA and dsRNA, and transduce signals leading to the production of IFN. Recently discovered cytoplasmic RNA helicases, RIG-I and MDA5, selectively sense viral RNA species. Gene disruption studies revealed the critical but non-redundant function of RIG-I and MDA5 in host antiviral responses.

Keywords: Interferon; RNA helicase; Innate immunity; TLR; Double-stranded RNA

1. Introduction

The expression of type I IFN (IFN-α, -β) gene is tightly regulated. IFN genes are virtually silent under normal conditions; however, when cells are appropriately stimulated such as by viral infection, they are turned on rapidly and after several hours of IFN secretion, they return to the dormant state [1]. Recently identified type III IFN (IFN-λ) genes, which are evolutionarily distinct from type I IFN, are similarly regulated by extracellular stimuli [2,3]. The function of type I IFN promoter was extensively studied in the 80's and critical *cis*-elements and interacting trans-acting factors were identified. IFN-α and -β gene promoters share common motifs [4,5], which bind to interferon regulatory factors (IRFs) [6]. IFN-β is additionally regulated by NF-κB and ATF2/c-Jun transcription factors [7–9]. In the late 90's, it was discovered that IRF-3 and IRF-7 have a critical function in IFN gene regulation [10–16]. Both IRF-3 and IRF-7 are activated by phosphorylation on specific serine residues.

2. IFN inducers and viral sensors

Although the activation mechanisms of transcription factors that regulate IFN genes were well elucidated by the end of the 90's, the initial detection of viruses by cells has been elusive. For a long time, protein kinase activated by RNA (PKR) was considered a likely candidate for a viral sensor because PKR is activated by double-stranded RNA, which is known to induce IFN; however, the analysis of knockout mice revealed that PKR is dispensable for IFN production [17]. Furthermore, several lines of evidence suggested that TBK-1 and IKK-i are kinases responsible for the phosphorylation and activation of IRF-3 and IRF-7 [18–22], indicating that separate molecules are responsible for viral sensing and regulatory phosphorylation, respectively.

Screening for IFN-inducing compounds was carried out in the 60's and 70's, identifying dsRNA such as poly (rI): poly (rC) and bacterial endotoxin along with various viruses. In the 90's, the function of Toll-like receptors (TLRs) in mammals was elucidated [23]. Nearly ten human and mouse TLRs detect various pathogen-associated molecules. TLR4 and TLR3 detect extracellular LPS and dsRNA, respectively, and lead to the activation of IFN genes [24–26] (Fig. 1). TLR3 transmits a signal to an adaptor, TRIF, and then activates TBK-1 and IKK-i [27–30]. TLR4 uses an additional adaptor TRAM, to signal the common cascade through TRIF [31–34]. These discoveries explain how LPS and dsRNA trigger the activation of IFN genes and lead to the speculation that TLR3 detects viral dsRNA in infected cells; however, cells defective for TLR3 normally activate IFN genes [35], suggesting alternative cytoplasmic sensor molecule(s).

* Corresponding author. Tel.: +81 75 751 4031.
E-mail address: tfujita@virus.kyoto-u.ac.jp (T. Fujita).

0300-9084/$ - see front matter © 2007 Elsevier Masson SAS. All rights reserved.
doi:10.1016/j.biochi.2007.01.013

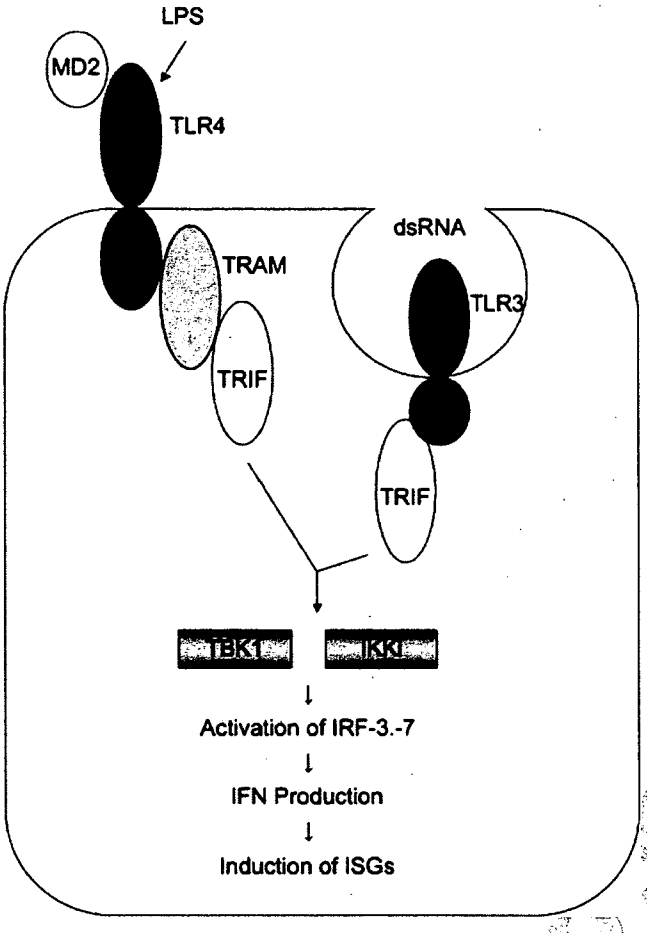

Fig. 1. Detection of LPS and dsRNA by TLR4 and TLR3. LPS and dsRNA, which are known as representative non-viral inducers of IFN production, activate the MyD88-independent signaling cascade as indicated. The two signaling cascades converge at signaling kinases, TBK-1 and IKK-I, which are responsible for the activation of transcription factors IRF-3 and -7, and the subsequent production of IFN.

3. RIG-I

Screening of an expression cDNA library, based on IFN promoter stimulation, identified a clone encoding RNA helicase, termed retinoic acid-inducible gene-I (RIG-I) [35]. The predicted structure of RIG-I is characteristic of N-terminal caspase recruitment and activation domain (CARD)-like structure and C-terminal DExD/H box RNA helicase domain. The N-terminal portion, which encompasses two CARD repeats and corresponds to the isolated clone by screening, acted as a dominant activator capable of inducing IFN production without viral infection. Full-length RIG-I, in contrast, exhibited low constitutive activity; however, when induced by viral infection, a marked augmentation was observed. These results suggest that CARD is responsible for signaling the downstream cascade, and the helicase domain strictly regulates CARD in a virus-dependent manner. Mutagenesis studies revealed that disruption of the ATP binding site within the helicase domain rendered RIG-I to a dominant inhibitor of virus-induced signal. Furthermore, the C-terminal 190 amino acid region is capable of inhibiting the RIG-I-mediated activation of IFN gene expression [36]. This internal repression domain physically interacts with the helicase domain, likely forming a "closed" or "constrained" structure to mask CARD (Fig. 2). Upon binding to dsRNA and presumably in the presence of ATP, RIG-I changes its conformation to expose CARD. Experiments using siRNA and cells derived from RIG-I knockout mice revealed that RIG-I is essential for IFN gene activation in different cells including myeloid dendritic cells (mDC), whereas plasmacytoid dendritic cells (pDC), specialized for massive IFN-a production, use distinct sensors, TLR7/8 and TLR9 [37] (see below).

In death signaling, CARD of Apaf I specifically interacts with that of caspase 9 to initiate apoptosis [38], thus these domains determine specificity and the direction of signaling. As expected, the downstream molecule of RIG-I also contains CARD (Fig. 2). Three laboratories independently identified this molecule from the database through CARD homology to MDA5, the closest relative of RIG-I (see below), termed MAVS, VISA and Cardif [39–41]. One group identified this protein by functional screening, and named it IPS-1 [42]. We refer to this protein as IPS-1throughout this article. IPS-1 localizes on the mitochondrial outer membrane through its C-terminal transmembrane domain and this localization is crucial for its function [39,43–45]. RIG-I interacts with IPS-1 through CARD/CARD interaction. Although TBK-1 and IKK-i are logical targets for IPS-1 signaling, its interaction with these kinases is controversial. Also, the role of mitochondria in IFN induction is elusive.

4. MDA5 and LGP2

Three presumptive helicases related to RIG-I are encoded in the human and mouse genome. MDA5 is the closest relative of RIG-I and exhibits amino acid sequence identity of 23% and 35% in CARD and the helicase domain, respectively. Functional studies using cell culture revealed that MDA5 positively regulates IFN genes in a similar fashion as RIG-I [46]; however, gene disruption studies showed that RIG-I and MDA5 sense different viral species [47,48]. RIG-I is essential for detecting influenza virus, Sendai virus, VSV and Japanese encephalitis virus (JEV), whereas the absence of MDA5 virtually unaffected IFN response by these viruses. Instead, MDA5 is essential for sensing encephalomyocarditis virus (EMCV), Mengo virus and Theiler's virus, all of which belong to the picornavirus family. Interestingly, the differential detection of these viruses is likely due to differences of viral RNA, since RNA extracted from the VSV virion is specifically detected by RIG-I. Another line of evidence is that dsRNA prepared by the transcription of various templates in vitro and poly (rI): poly (rC) are detected by RIG-I and MDA5, respectively. Although the chemical basis of the differential detection of these RNA is poorly understood, recent reports shed some light on self and non-self RNA discrimination (see below).

The third member of the helicase family is LGP2, which exhibits 31% amino acid identity to RIG-I in the helicase